TURUN YLIOPISTO

Expression, purification, and characterisation of a novel bacterial ADP-ribosyltransferase

Molecular Biosciences (Biochemistry)

Pro gradu thesis

Author:

Abdula Habib

22.5.2023

Turku

Pro gradu thesis

Subject: Molecular Biosciences (Biochemistry)
Author: Abdula Habib
Title: Expression, purification, and characterization of a novel bacterial ADP-ribosyltransferase
Supervisor: Dr. Arto Pulliainen
Number of pages: 68 pages
Date: 22.5.2023

ADP-ribosylation is a chemical modification that is mostly known as a post-translational modification targeting nucleophilic amino acid residues. It utilizes the common coenzyme NAD^+ as the reactant. The reaction is catalysed by ADP-ribosyltransferases (ARTs) which include bacterial AB-exotoxins also known as bARTTs (bacterial ART toxins). Exotoxins are proteins with enzymatic activity that are secreted or released upon lysis. They are secreted by pathogenic bacteria such as *Corynebacterium diphtheria* and *Vibrio cholerae*.

Previously the Turku Cellular Microbiology Laboratory has discovered *in silico* open reading frames from different *Bartonella* species. The aim of my thesis is to express, purify and functionally characterise a putative open reading frame from *Bartonella sp. 1-1C* named CtxA. The N-terminally hexahistidine tagged CtxA constructs are transformed into an *E. coli* expression strain and purified with nickel-nitrilotriacetic acid (Ni-NTA) affinity chromatography followed by size-exclusion chromatography (SEC). The auto- and trans-ADP-ribosylation activity is studied with western blot assays. As a result of my studies the proteins were successfully purified and verified with anti-His western blot. Furthermore, both anti-MAR/PAR and biotin-ADP-ribose streptavidin western blots suggest that CtxA is a novel bARTT with auto-ADP-ribosylation activity. The target substrate for CtxA was not found despite the promising results from eukaryotic lysate studies.

Key words: ADP-ribosylation, exotoxin, NAD^+

Table of contents

Abbreviations

ADPr	adenosine diphosphate ribose
AIM	auto-induction medium
ART	ADP-ribosyltransferase
ARTT	ADP-ribosyltransferase turn-turn motif
bARTT	bacterial ADP-ribosyltransferase toxin
CT	cholera toxin
DSF	differential scanning fluorometry
DT	diphtheria toxin
ER	endoplasmic reticulum
ERAD	ER-associated degradation pathway
EXE	glutamate-X-glutamate motif
HYE	histidine-tyrosine-glutamate motif
IMAC	immobilized metal-affinity chromatography
LT	heat-labile enterotoxin
MAR	mono-ADP ribose
MSA	multiple sequence alignment
MUT	mutated protein
NAD^+	nicotinamide adenine dinucleotide
Ni-NTA	nickel-nitriloacetic acid
PAR	poly-ADP ribose
PE	exotoxin A
PT	pertussis toxin
PTM	post-translational modification

RFU	relative fluorescence unit
RSE	arginine-serine-glutamate motif
RT	room temperature
SEC	size exclusion chromatography
S_N1	unimolecular nucleophilic substitution reaction
S_N2	bi-molecular nucleophilic substitution reaction
SOL	soluble cell lysate
STS	serine-tyrosine-serine motif
TOT	total cell lysate
TRUNC	N- and C-terminal truncated protein
WT	wildtype protein

1 Review of literature

1.1 ADP-ribosylation

ADP-ribosylation is an ancient reversible reaction found in all forms of life. It is catalysed by ADP-ribosyl transferases (ARTs) that transfer adenosine diphosphate ribose (ADPr) moieties from the coenzyme nicotinamide adenine dinucleotide (NAD^+) to the target substrates while nicotinamide is cleaved off (Figure 1). (Lüscher et al. 2021.) ADP-ribosylation is mostly known as a post-translational modification (PTM) targeting amino acids with nucleophilic residues such as aspartate, glutamate, lysine, arginine, cysteine, and threonine. However, it cannot be considered solely as a PTM after the discovery of its role in modifying nucleic acids such as transfer RNAs (Culver et al. 1993; Spinelli et al. 1999) as well as single stranded DNAs (Jankevicius et al. 2016) and double stranded DNAs (Takamura-Enya et al. 2001). ADP-ribosylation can also modify small-molecule antimicrobials (Dabbs et al. 1995).

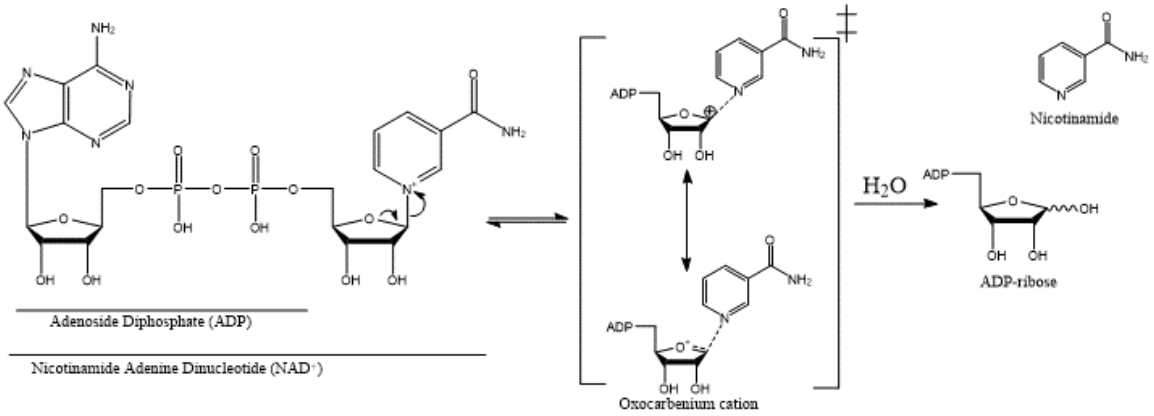

Figure 1. Basic chemistry of the NAD^+ hydrolysis reaction. *NAD^+ is relatively unstable because of its positively charged nicotinamide moiety that acts as a weak base. The nucleophilic oxygen attacks the anomeric carbon resulting in a resonance-stabilized transition state, an intermediate called oxocarbenium cation. The dashed line between the cation and nicotinamide indicates that the moiety is about to be cleaved off. The transition state is stabilized by a nucleophilic attack on the anomeric carbon by H_2O in the case of auto-hydrolysis, which many ARTs demonstrate, or with the incoming substrate amino acid rendering ADP-ribose. The figure was generated with ChemDraw 6.0.*

ADP-ribosylation is also a key reaction utilised by many pathogenic bacteria through the secretion of exotoxins (Simon et al. 2014). The first exotoxin that was proven to have ART activity was the diphtheria toxin (DT) of *Corynebacterium diphtheriae* (Goor et al. 1967). Following this discovery many other ADP-ribosylating toxins were found. The earliest found and most studied toxins are cholera toxin (CT) of *Vibrio cholerae* (Cassel and Pfeuffer 1978), heat-labile enterotoxin (LT) of *Escherichia coli* (Moss and Richardson 1978), exotoxin A (PE) of *Pseudomonas aeruginosa* (Pavlovskis et al. 1978), and pertussis toxin (PT) of *Bordetella pertussis* (Katada and Ui 1981). The most conjunctive factor of these toxins is that they belong to the AB-like proteins where A is the ADP-ribosylating subunit and the B subunit is utilized in receptor binding and translocating the toxin inside the cell (Domenighini et al. 1994).

ARTs are divided into two main groups based on the amino acids located in the active site: diphtheria toxin-like (DT-like) and cholera toxin-like (CT-like) (Simon et al. 2014). The first group is characterized by its active site motif HYE consisting of a His, two Tyr and one Glu residue (Carroll and Collier 1984, 1987, 1988). The second group has an RSE (Arg-Ser-Glu) motif, which also catalyses the mono-ADP-ribosylation (MARylation) reaction (Domenighini et al. 1994).

1.1.1 Mono ADP-ribosylation

MARylation is the attachment of one ADPr to the target substrate. It is the most prevalent form of ADP-ribosylation found originally as a way of function of the diphtheria toxin by Honjo et al. (1968). The group was first to discover that DT MARylates a modified histidine residue 2-[3-carboxy-amido-3-(trimethylammonio)propyl]-histidine, commonly known as diphthamide of the eukaryotic elongation factor 2 (eEF2), thus inhibiting protein synthesis in the host cell.

Many other bacterial toxins have MARylation activity (Table 1). There are at least five bacterial ADP-ribosylating toxin (bARTT) groups according to structure-function organization and the nature of their target (Simon et al. 2014). eEF2 targeting DT (Choe et al. 1992) and PE (Allured et al. 1986) are both large single chain AB proteins with receptor binding, transmembrane targeting, and protease-resistant catalytic domains. The most well-known toxins CT, PT and LT have AB_5 structural composition, and they target small regulatory G-proteins (Sixma et al. 1991; Stein et al. 1994; Zhang et al.

1995). The third group is actin-targeting AB binary toxins where the A and B domains are secreted independently and interact with one another on the surface of the host cell. This group includes a myriad of clostridial toxins such as CDT of *Clostridium difficile.* (Perelle et al. 1997; Gülke et al. 2001.) Another group similar to this is the collection of exoenzymes, the proteins of which only contain the ADP-ribosylating A subunit (Wilde et al. 2003). Here the need for a B subunit is obsolete because bacteria secreting effector molecules such as ExoS (Pederson et al. 1999) and SpyB (Lesnick et al. 2001) utilize the type III secretion system for toxin delivery. The last bARTT group consist of toxins with novel structures such as the typhoid toxin (TT) which has a structure composition of $2AB_5$. The 2A is a dual-activity protein with a DNAase domain and an ADP-ribosylating domain. Although the exact eukaryotic target protein for TT has not yet been identified, it prefers disialoganglioside GD2, which indicates that the B subunit of TT may use glycolipids as receptors. (Song et al. 2013.)

Table 1. Examples of bacterial ADP-ribosyltransferase toxins

Exotoxin	**Bacterium**	**AB structure**	**Eukaryotic target**	**ADP-ribosylated amino acid**	**Role in pathogenesis**
Diphtheria toxin (DT)	*Corynebacterium diphtheria*	AB	EF2	Diphthamide (modified histidine)	Inhibition of protein synthesis
Exotoxin A (PE)	*Pseudomonas aeruginosa*	AB	EF2	Diphthamide	Inhibition of protein synthesis
Cholera toxin (CT)	*Vibrio cholerae*	AB_5	G_{as}	Arginine	Inhibition of GTPase activity
Pertussis toxin (PT)	*Bordetella pertussis*	AB_5	G_{ai}	Cysteine	G protein signalling disruption
Heat-labile enterotoxin (LT)	Enterotoxigenic *Escherichia coli*	AB_5	G_{as}	Arginine	Inhibition of GTPase activity
CDT	*Clostridium difficile*	A B	Actin	Arginine	Prevention of actin polymerization
ExoS	*Pseudomonas aeruginosa*	A	Ras, vimentin	Arginine	Disruption of actin microfilaments
SpvB	*Salmonella enterica*	A	Actin	Arginine	Prevention of actin polymerization
Typhoid toxin (TT)	*Salmonella enterica sp. Typhi*	$2AB_5$	Unknown	Unknown	Unknown

In most cases, the targets of bARTTs are key regulators of cellular function. Interference in their activity, caused by MARylation, leads to serious deregulation of crucial cellular processes leading to eventual cell death (Figure 2). (Simon et al. 2014.) All in all, a rough generalization can be made of bARTT toxin groups. DT-like toxins are involved in the modulation of protein synthesis machinery whereas CT-like toxins are implicated in intracellular trafficking, actin cytoskeleton modulation and G protein modification. (Roussin and Salcedo 2021.)

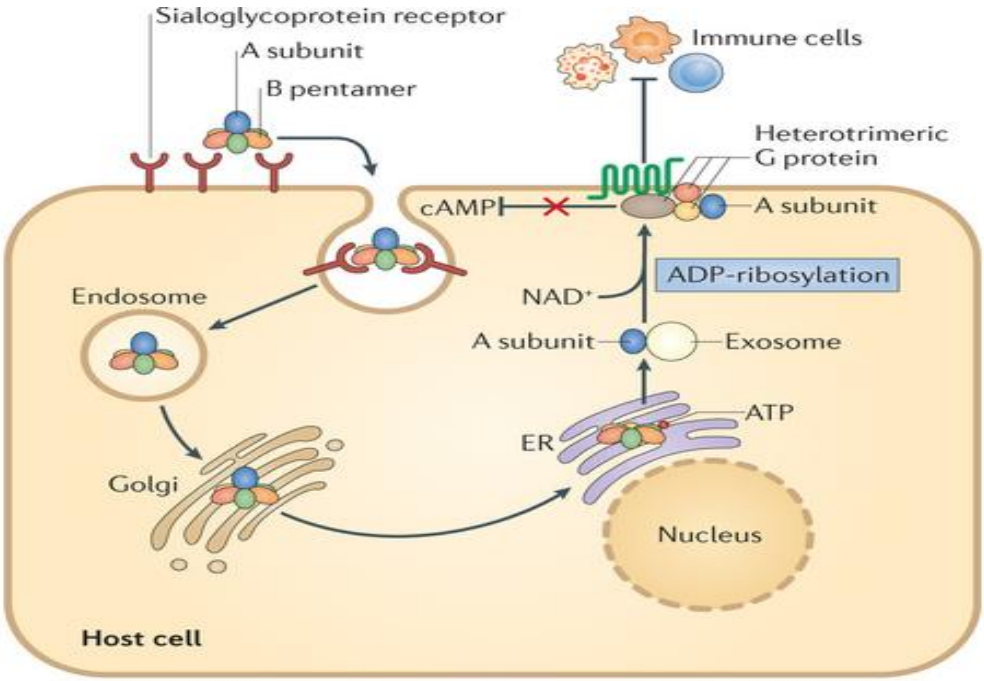

Figure 2. Function of the pertussis toxin (PT). *PT comprises a heteropentameric B subunit with receptor binding capabilities and an ADP-ribosylating A subunit that is non-covalently bound to the B subunit. Here, the B subunit of PT recognizes sialoglycoprotein receptors on the surface of the eukaryotic host cell, and the toxin is endocytosed via clathrin-coated pits. It then accumulates in coated vesicles and larger intracellular compartments, namely, the endosome. After that, it is suggested that the toxin follows the retrograde transport system involving the Golgi apparatus and the endoplasmic reticulum (ER). In the ER, the B subunit is glycosylated which destabilizes the interaction between subunits A and B. Hence, the A subunit dissociates from the B subunit and is reduced by disulphide isomerases found in the ER before it is translocated to the cytosol. Cytosolic, reduced A subunit catalyses the transfer of an ADP-ribose moiety onto acceptor substrate proteins. The acceptor substrates are the α*

subunits of signal transducing heterotrimeric G proteins. To be precise, PT ADP-ribosylates the cysteine residue 351 of G_i and G_o. ADP-ribosylation of this residue results in the uncoupling of the G protein from its cognate receptor and the disruption of signal transduction. This has many outcomes, the induction of lymphocytosis being one. (Pescador Vargas and Roa Culma 2017)

1.1.2 Poly ADP-ribosylation in bacteria

Poly ADP-ribosylation (PARylation) is the attachment of multiple ADPrs to the target substrate. It was first discovered in acid-insoluble nuclear extracts in 1963 (Chambon et al. 1963). PARylation is generally seen in higher eukaryotes. It is involved in cellular processes, including gene expression, cellular signalling, cell cycle progression, DNA repair, apoptosis, and necrosis. The enzymes belonging to this family are called poly-ADP-ribose polymerases (PARPs). (Perina et al. 2014.)

Some bacterial species are found to have PARP gene homologs even though bacteria are thought to lack poly-ADPr metabolism. It is postulated that bacteria acquired their PARP genes through horizontal gene transfer. (Perina et al. 2014.) The most compelling evidence that prokaryotes may have PARPs is the detection of endogenous PARylation activity in *Deinococcus Radiodurans*. However, the role of PARylation in *D. radiodurans* is not clear. It may be involved in DNA damage response similarly to PARP1 in eukaryotes. (Cho et al. 2019.) It must also be noted that no PARP homologs can be found in the genome of *D. radiodurans*. (Perina et al. 2014; Cho et al. 2019.) Interestingly, PARylation activity does not necessarily mean the enzyme responsible belongs to PARPs as some mono ADP-ribosyltransferases can generate ADPr chains (Morrison et al. 2006). Thus, in the case of *D. radiodurans*, there may be a highly divergent PARP that is yet to be discovered. Alternatively, enzymes with known ART activity may act as alternative PARPs. (Cho et al. 2019.)

In vitro PARP activity has been linked to two bacterial PARP homologs from *Herpetosiphon aurantiacus* (HaPARP) (Slade et al. 2011) and *Clostridioides difficile* CD160 (CdPARP) (García-Saura et al. 2018). HaPARP is highly sensitive to PARP inhibitor and requires DNA for its activity, a characteristic that is in line with human PARPs (Slade et al. 2011). Both HaPARP and CdPARP reactions were reversible by PAR-

glycohydrolases, enzymes that remove ADPrs from the target substrate (Slade et al. 2011; García-Saura et al. 2018).

1.2 Structure and function of bARTTs

bARTTs have diverse functions in pathogenesis which they achieve through the ADP-ribosylation of various substrates (Simon et al. 2014). Although these toxins modify numerous target proteins and share low sequence identity (Figure 3), their crystal structures have similar overall three-dimensional structures and highly conserved NAD^+-binding pockets. The focus of this chapter will be on the structure and function of the A subunit of bARTTs as it alone is responsible for the ADP-ribosylation activity.

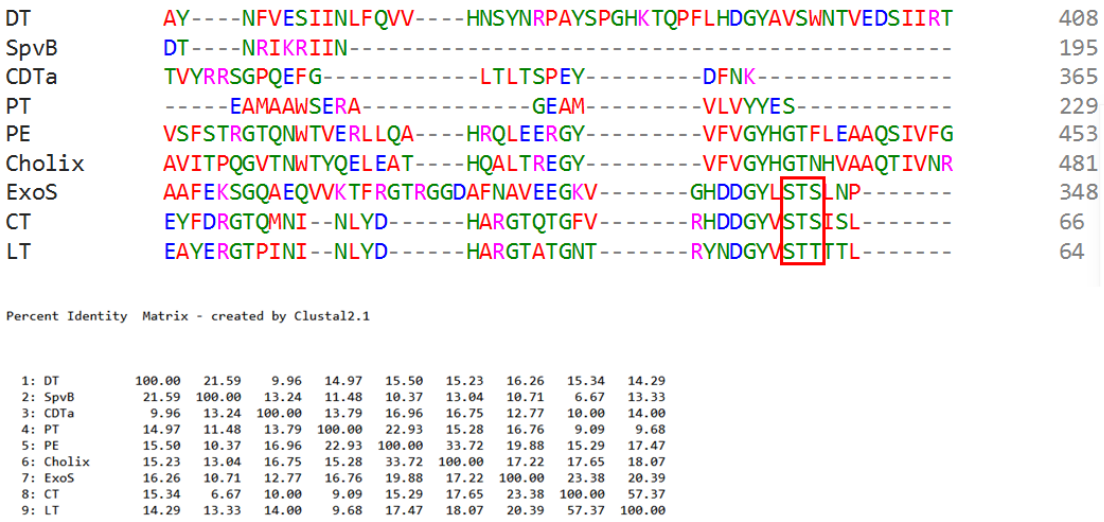

Figure 3. Multiple sequence alignment (MSA) of bARTTs. *A characteristic of ARTs is that they may have low sequence identity despite belonging to the same enzyme family. Namely, the MSA of primary amino acid sequences does not provide accurate information about the evolutionary relations between the different toxins. Despite this, some conservation patterns can be seen such as the STS motif important for NAD^+ binding. The most closely related toxins CT and LT share 57 % sequence identity whereas ExoS, also belonging to CT-like toxins has 23 % sequence identity with CT and 20 % sequence identity with LT respectively. The MSA was generated with Clustal Omega 1.2.4.*

1.2.1 The conserved catalytic domain of bARTTs

Because of very poor primary structure conservation, bARTTs are recognised by their catalytic cleft which has three short, conserved regions. The consensus sequence of the region differs between the DT-like and CT-like toxins (Figure 4). (Domenighini et al. 1994; Masignani et al. 2003, 2004.)

Figure 4. MSA of the well-studied DT-like and CT-like toxins based on the tertiary structure of the catalytic core of their A subunit. *DT (PDB: 1F0L), PE (PDB: 1IKQ), and Cholix toxins (PDB:2Q5T) have a HYE catalytic region. CT-like toxins such as CT (PDB: 1XTC), LT (PDB: 1TII), and PT (PDB: 1PRT) have an RSE catalytic region. The structural alignment was generated with VAST* (Gibrat et al. 1996)

The first region has nucleophilic amino acids, either His (H) in the DT group or Arg (R) in CT group of toxins. In the DT group the motif is Tyr-His (YH) while CT group may have aliphatic residues such as Val (V) or Leu (L) before the aromatic residue and the nucleophilic residue (V/LYR) (Domenighini et al. 1994.) The exact role of Arg/His is toxin dependent. In DT, His forms a hydrogen bond with one of the hydroxyl groups on

the adenine ribose ring during the ADP-ribosyltransferase reaction. It also forms a bond with the backbone carbonyl of one of the Tyr residues in region 2. Through this bond, the Tyr is orientated into the correct conformation to bind the NAD^+. (Bell and Eisenberg 1997.) In PE and Cholix toxins the His residue also plays a role in the catalysis of ADP-ribosylation through its interaction with NAD^+ (Han and Galloway 1995; Jørgensen et al. 2008). Arg in CT, LT, and PT is not directly involved in binding NAD^+ but instead it supports key parts of the active site. The purpose of the Arg residue is to give structural integrity to the active site without being directly involved in reaction catalysis. Despite not being directly involved in catalysis, mutating the Arg residue results in significant loss of enzymatic activity. (Burnette et al. 1988, 1991; Lobet et al. 1991.)

The second region, Y-x_{10}-Y in the DT-like group and Ser-Tyr-Ser (STS) in the CT-like group, displays the major difference in the catalytic sites between the two toxin groups. The Tyr residue is vital for DT activity, and it is one of the two conserved Tyr residues essential for NAD^+ binding through aromatic ring π-orbital stacking. This is also the case regarding PE and Cholix toxin (Li et al. 1996; Jørgensen et al. 2008). Aromatic ring stacking may explain the slightly different conformations that NAD^+ possesses in the DT-like group bARTTs compared to those in the CT-like group (Dolan et al. 2000). STS (STT in LT) makes up part of the NAD^+ binding cavity of the CT-like toxins. It follows the amino acid pattern aromatic-hydrophobic-STS. (Domenighini and Rappuoli 1996.) Like Y-x_{10}-Y of the DT-like toxins, STS plays a similar role, stabilizing and maintaining the structure of the active site (Dolan et al. 2000).

The third region of the catalytic site has a strictly conserved catalytic Glu residue found in both the DT- and CT-like group of bARTTs. The catalytic Glu is part of the Gln/Glu-X-Glu motif (Q/EXE) in the CT-like group where X represents any amino acid residue. The Glu residues in both toxin groups are located in identical positions within the active site cleft, laying opposite to the Arg/His residue. (Masignani et al. 2004.) Naturally, all the aforementioned regions are interconnected and in the next section I will further elucidate the three-dimensional structure of the catalytic cleft.

1.2.2 Three-dimensional structure of the catalytic cleft of bARTTs

Both the DT-like and the CT-like group of bARTTs possess an active site with an α/β structure 70 – 100 amino acid residues in length (Han and Tainer 2001). The bARTT NAD^+-binding core consist of two perpendicular β-sheets with a variable number of α-helices both below and above the frame of β-sheets (Figure 5) (Domenighini et al. 1994). In addition, both toxin groups have an active site loop called ADP-ribosyltransferase turn-turn (ARTT) that is vital for substrate binding. The catalytic Glu residues of the toxin groups are part of ARTT. (Han and Tainer 2001.) The ARTT loop becomes disordered and undergoes conformational changes during NAD^+ binding (Li et al. 1996; Bell and Eisenberg 1997).

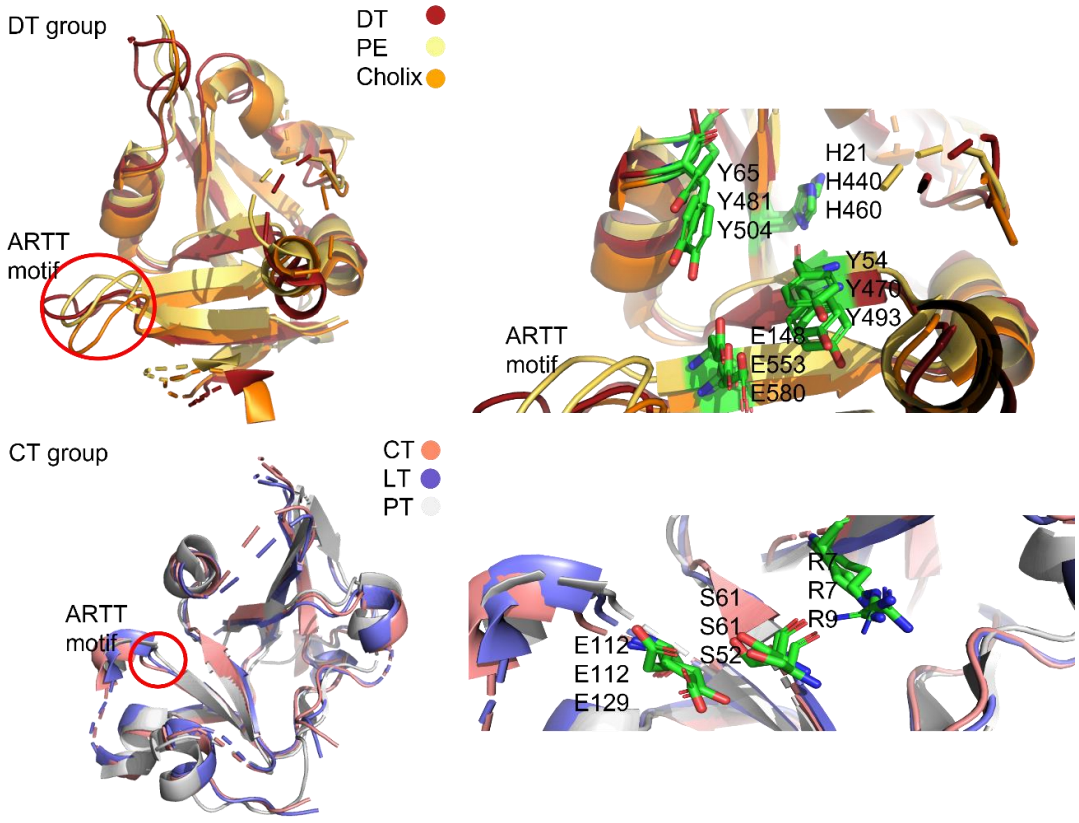

Figure 5. The structure of the active site of the DT-like and the CT-like group of bARTTs. *The superimposed structures in the DT-like group are DT in firebrick (PDB: 1F0L), PE in yellow orange (PDB: 1IKQ) and Cholix in orange colour (PDB: 2Q5T). The structurally and catalytically important amino acids which form the so-called HYE motif are shown: H21 in DT, H440 in PE and H460 in Cholix. The two conserved Tyr residues of Y-x_{10}-Y are Y54 and Y65 in DT, Y470 and Y481 in PE and Y493 and Y504 in the Cholix toxin. The catalytic Glu residues are E148 in DT, E550 in PE, and E580 in Cholix. In the*

CT-like group, CT is shown in salmon (PDB: 1XTC), LT in slate blue (PDB: 1TII), and PT in white colour (PDB:1PRT). The amino acids of the RSE catalytic motif are R7 in CT and LT, R9 in PT, S61 in CT and LT, S52 in PT, E112 in CT and LT and E129 in PT. Overall, only the conserved amino acids are displayed in the structures. The dashed lines shown indicate that the missing amino acids are not conserved between the toxins. The ARTT motif is shown in both toxin groups. This motif undergoes conformational changes during reaction catalysis. Figures were generated with PyMOL 2.4.1 (Schrodinger, LCC)

1.2.3 The catalytic mechanism of bARTTs

The conservation of the NAD^+-binding site and the amino acids involved in reaction catalysis suggests that a similar reaction mechanism takes place in a slightly different fashion between the DT-like and CT-like toxins. In general, the anomeric carbon of NAD^+ is susceptible to nucleophilic attack because of the electronegative atoms surrounding it causing electron depletion. In the absence of the substrate, the anomeric carbon is attacked by water molecules, hence the NAD^+ is hydrolysed. In the presence of the substrate, its nucleophilic amino acid attacks the anomeric carbon and forms a transition state. This is eventually resolved by transferring ADPr to the substrate molecule. The catalytic Glu interacts with the substrate by either guiding the approach of the nucleophilic amino acid or by participating in the formation of the transition state. (Domenighini et al. 1994.)

It is proposed that the reaction mechanism in DT-like and CT-like toxins is either S_N1 or S_N2 nucleophilic substitution (Domenighini and Rappuoli 1996). In the S_N1 reaction mechanism the nicotinamide leaves first with the generation of a reactive oxocarbenium ion as an intermediate which is attacked by the target substrate. The positively charged oxocarbenium intermediate i.e., the transition state is stabilized by the catalytic Glu (Q/EXE motif) and the formed ADPr remains bound to the active site. (Sixma et al. 1991; Bell and Eisenberg 1997.) In this case, the oxocarbenium intermediate is directly stabilized through the electrostatic forces of the catalytic Glu and the hydroxyl group of Ser found in the conserved STS motif (Locht and Antoine 1995). For the DT group, which does not possess an STS motif, the ARTT loop could position the target substrate for nucleophilic attack on the positively charged oxocarbenium intermediate. The attack from the nucleophilic substrate releases the

ADPr from the active site to the target substrate. (Li et al. 1996; Bell and Eisenberg 1997; Jørgensen et al. 2008.)

In contrast, if an S_N2 reaction occurs, the activated nucleophile attacks the anomeric ring on NAD^+ and associates with the leaving nicotinamide. This leads to steric hindrance as there would be no space for the catalytic Glu (Q/EXE motif) to stabilize the forming oxocarbenium intermediate. In an S_N2 reaction, a stable oxocarbenium intermediate is not formed but rather a nicotinamide ribose diol which can then be stabilized through the catalytic Glu residue. (Locht and Antoine 1995.) The main difference between the S_N1 and S_N2 reactions in this case is whether a true oxocarbenium intermediate or an oxocarbenium-like intermediate, such as the nicotinamide ribose diol, is formed (Figure 6). Although biochemical data supports the S_N1 reaction mechanism as a way of action for both the DT-like and CT-like toxins, the S_N2 reaction seems more probable for some individual toxins albeit kinetic studies not generally supporting this hypothesis (Locht and Antoine 1995; Scheuring and Schramm 1997).

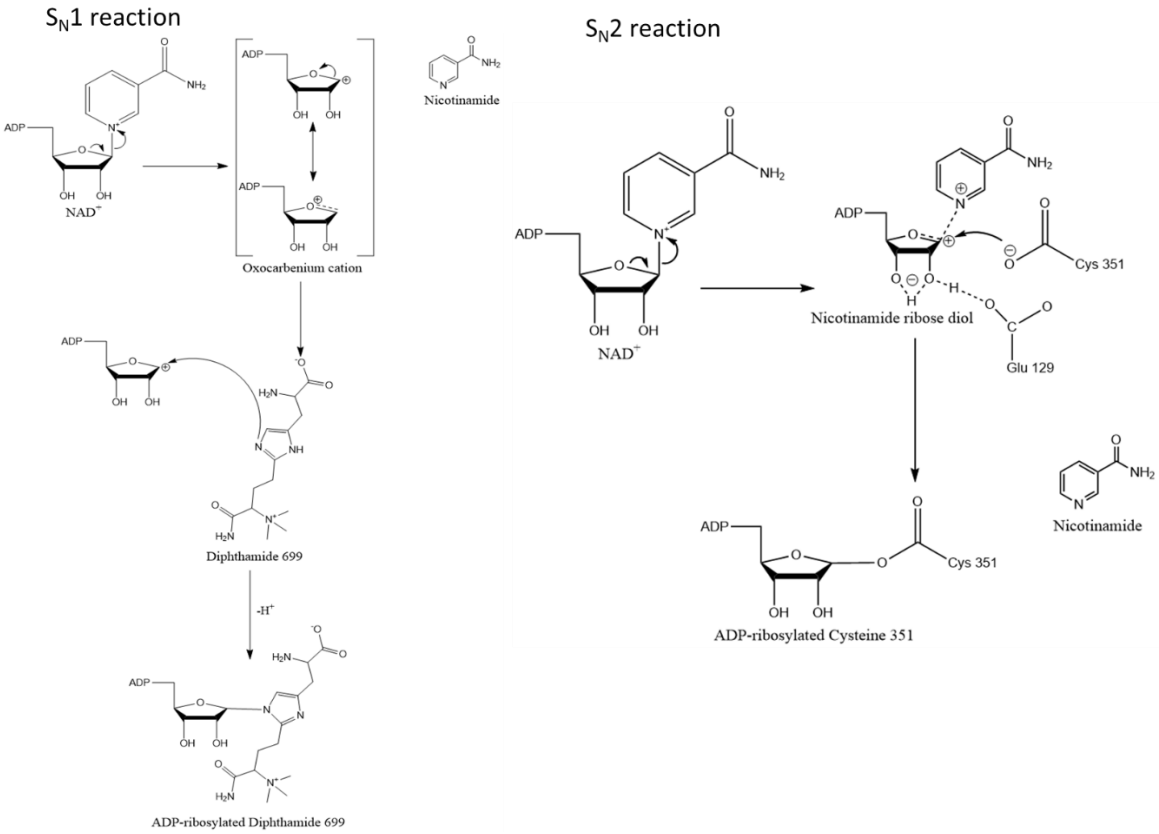

Figure 6. A simplified model of the ADP-ribosylation reaction mechanism of DT and PT*. In the S_N1 reaction, an oxocarbenium cation is formed and held in the catalytic site*

while nicotinamide is cleaved off. The cation is then subjected to a nucleophilic attack from the incoming target substrate, such as the post-translationally modified histidine 699 of eEF2, and an N-glycosidic bond is formed. However, in the S_N2 reaction, nicotinamide ribose diol, an oxocarbenium-like intermediate is formed via interaction with the invariable glutamate. The cysteine 351 of Gα attacks the formed intermediate, relieving the transition state and forming an O-glycosidic bond. The figures were generated according to Locht and Antoine (1995) *and Jørgensen et al.* (2005).

It must be noted that no generalizations can be made regarding the catalytic nature of the DT-like and CT-like toxins. To understand the bigger picture, each toxin must be seen as an entity with its own characteristics. This holds true especially in the case of the CT-like toxin group. For example, the subgroup of CT-like toxins such as C2 binary toxins and C3 exoenzymes have unique structural and catalytical characteristics that will not be covered in this thesis.

1.2.4 Function of the DT-like group of bARTTs

The DT-like group is limited to only three toxins (DT, PE, and Cholix) that all ADP-ribosylate diphthamide 699 on eEF2 (Jørgensen et al. 2008). Generally, these toxins are organized as single polypeptides having three structural domains called the catalytic (C), the transmembrane or translocation (T) and the receptor-binding (R) domains. In this case, according to AB denomination, C corresponds to the catalytic A subunit while T and B are part of the receptor binding B subunit. (Gillet and Barbier 2015.)

During the intoxication of a cell with DT, the toxin binds to its cellular receptor which is a precursor of heparin-binding epidermal growth factor (HB-EGF) called proHB-EGF (Naglich et al. 1992). The cellular receptor of PE on the other hand is the α2-macroglobulin receptor/low-density lipoprotein receptor-related (LRP) protein (Kounnas et al. 1992). This is also the case for the Cholix toxin. In addition, Cholix is able to intoxicate cells deficient in LRP, indicating that it can recognize other still unidentified cell surface receptors. (Jørgensen et al. 2008.)

After receptor recognition, the toxins must be proteolytically activated. In DT a 14 amino acid signal peptide between the C and T domains is cleaved by a cellular protease called furin (Figure 7) (Tsuneoka et al. 1993). PE is cleaved by a furin-like

protease that recognizes the amino acid sequence RQPR (Chiron et al. 1994; Inocencio et al. 1994). Since Cholix shares structural similarity to PE, there is a possibility that it is also activated by furin or a furin-like protease (Fieldhouse et al. 2012). The toxins are then internalized. In the case of DT, the clathrin-coated pathway takes in the cleaved C-T-complex through endosomal membranes (Lemichez et al. 1997). The pH shift in the endosomes changes the conformation of the T domain (Chenal et al. 2002). Thus, the T domain assists in translocating the C domain across the endosomal membranes to the cytosol (Lemichez et al. 1997).

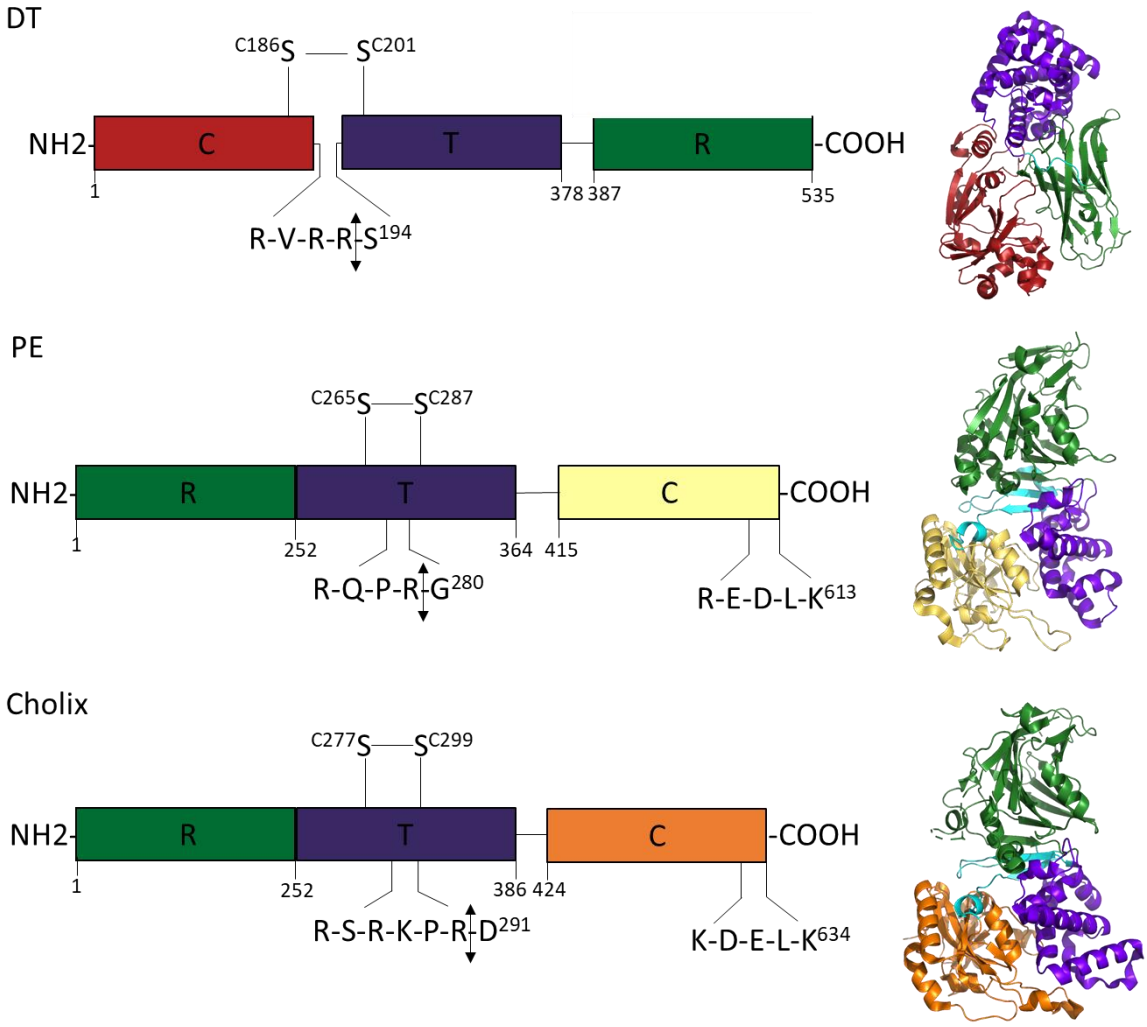

Figure 7. Structural organization of DT, PE and Cholix and their three-dimensional structures. *The receptor binding domain (R) is displayed in forest green, translocation domain (T) in purple blue and the catalytic (C) domain with a unique colour. The linker domain between T-R and T-C is displayed in cyan. PE (PDB: 1IKQ) and Cholix (PDB: 2Q5T) have inversed structural organization to DT (PDB: 1F0L). The disulphide bridge (S*

– S) between Cys residues (Cxxx, where x is the numerical order of the amino acid in the sequence) important for reduction and protein activation as well as the arginine-rich furin protease sites are shown. The two-sided arrow indicates the cleavage site. In addition, PE and Cholix have a C-terminal signal sequence important for toxin trafficking inside the host cell. The figure was generated according to Gillet and Barbier (2015) *and* Jørgensen et al. (2008)*.*

PE as well as DT are also internalized through receptor-mediated endocytosis (Taupiac et al. 1996). In contrast to DT, PE undergoes retrograde trafficking through the Golgi apparatus to the ER (as is shown in the case of the PT toxin in Figure 2). This is mediated by an endosomal retrieval motif-like sequence found on the carboxyl-terminal (C-terminal) part of PE having an amino acid sequence REDLK (Chaudhary et al. 1990). The C-terminal signal sequence is cleaved off after which PE is transported from the early endosome to the ER (McKee and FitzGerald 1999). The C domain of PE is secreted from the lumen of the ER into the cytosol by Sec61, a complex that degrades improperly folded proteins (Gillet and Barbier 2015). This is more commonly known as the ER-associated degradation pathway (ERAD) (Simon et al. 2014). The precise internalization of Cholix is not known other than it moving through receptor-mediated endocytosis (Jørgensen et al. 2008; Fieldhouse et al. 2012).

During the translocation process the disulphide bond of the C-T complex needs to be reduced. This releases the C domain from the complex to the cytosol of the cell where it can function. The timing of the reduction of the disulphide bond is vital as too early of a reduction result in the loss of enzymatic activity. In DT, the reduction occurs just before the toxin is secreted from the endosomal membranes to the cytosol. (Falnes and Olsnes 1995; Ratts et al. 2003.) In PE the disulphide reduction occurs within the ER (McKee and FitzGerald 1999). Since Cholix shares similarity in all of its structural components with PE, this suggests that Cholix too needs to be reduced before it enters the cytosol (Jørgensen et al. 2008).

As the last the of ADP-ribosylation the C domain catalyses the transfer of ADPr from NAD^+ to its target substrate, the diphthamide 699 of eEF2. This blocks messenger RNA translocation within the ribosome complex and inhibits eukaryotic cell protein synthesis. (Gillet and Barbier 2015.) ADP-ribosylation of eEF2 is irreversible. In other

words, it cannot be reversed by any endogenous mechanisms in the cells. (Falnes et al. 2000.)

1.2.5 Function of the CT-like group of bARTTs

The CT-like group is voluminous as most bARTTs belong to this category (Simon et al. 2014). Because of this, only the function of CT, LT and PT will be covered. These toxins are multimeric polypeptides with a pentameric receptor binding B subunit and a dual-chain A subunit with a catalytic domain and a signal domain linking the A subunit non-covalently to the B subunit (Heggelund et al. 2015; Masin et al. 2015).

The cell surface receptor for CT, LT and PT is the GM1 ganglioside in the small intestinal epithelium (Holmgren et al. 1975, 1982; Armstrong et al. 1988). PT is a promiscuous enzyme, generally targeting sialoglycoproteins (Armstrong et al. 1988). It can also target other glucoconjugates such as glucolipids (Hausman and Burns 1993). After initial receptor binding and endocytosis, the toxins relocate to early and recycling endosomes (Iglesias-Bartolomé et al. 2009). From there they relocate to the trans-Golgi network. Interestingly, it seems that GM1 alone can transport the toxins to the Golgi and late endosomal compartments. (Chinnapen et al. 2012.) This is in sharp contrast to DT and PE which need a special signal sequence. It must be noted that both CT and LT possess a C-terminal signal sequence on their A subunit, KDEL in CT and RDEL in LT. It is thought that the signal sequence of CT and LT assists in the transport of the toxins from the Golgi apparatus to the ER, but that the sequence is not required for transportation. (Lencer et al. 1995.)

Before entering the ER, the dual-chain A subunit of CT and LT is cleaved into fragments A1 and A2 that are linked through a disulphide bond. In the ER, the disulphide bond is reduced. This reduction is catalysed by a chaperone in the ER called protein disulphide isomerase. (Majoul et al. 1997.) There are also other chaperones that help prevent the reduced A1 fragment from aggregating in the ER (Heggelund et al. 2015). The translocation of the A1 fragment from the ER to the cytosol is thought to occur through the Sec61 channel complex such as is the case with the PE toxin mentioned previously (Wiertz et al. 1996). An alternative method suggests that the chaperone Hsp90 interacts with the A1 fragment and transports it to the cytosol. In addition Hsp90 may help the toxins evade the ERAD pathway by preventing their

ubiquitination. (Taylor et al. 2010.) The role of Hsp90 in preventing toxin ubiquitination is unclear as the A subunits do not undergo ubiquitination due their lack of lysine residues (Hazes and Read 1997).

When released to the cytosol, the toxins are allosterically activated. In the case of CT, the host ADP-ribosylation factor ARF6 binds to the A1 fragment. This induces a conformational change that allows NAD^+ binding in the active site. (O'Neal et al. 2005.) Other factors such as lipid rafts in the host cell may take part in either activating or stabilizing the conformation of the A1 fragment (Ray et al. 2012). The activated toxin catalyses the transfer of ADPr from NAD^+ to Arg 201 in the Gs α-subunit. This leads to constitutive Gsα activation which in turn activates adenylyl cyclase (Moss and Vaughan 1977; Gill and Meren 1978). Adenylyl cyclase continuously produces a second messenger cyclic AMP (cAMP) from ATP. One of the targets of cAMP is protein kinase A (PKA) in the intestinal epithelial cells. PKA phosphorylates the membrane chloride channel cystic fibrosis transmembrane conductance regulator (CFTR). CFTR secretes Cl^- ions from the cells into the intestinal lumen. (Picciotto et al. 1992.) This upsets the electrolytic balance forcing positive ions such as Na^+ across the extracellular medium of the intestine. The increased salt concentration makes the environment hypertonic in the intestine which provides the osmotic pressure to force enormous amounts of water out of the cells, exceeding one litre per hour in secretory diarrhoea. Hence, the activation of the CFTR is the primary way by which CT and LT promote water efflux from the cells. (Heggelund et al. 2015.)

As for PT, it is generally thought to follow the same internalization pattern as CT and LT (Hazes and Read 1997) despite the toxin having a distinct structure (Figure 8). Once it reaches the cytosol, the A subunit of PT called S1 transfers the ADPr to Cys 351 in G_i and G_o α-subunits preventing their activation and coupling with G protein-coupled receptors (Masin et al. 2015). This has the opposite effect compared to CT and LT catalysed ADP-ribosylation. G_i and G_o mediated signalling pathways are switched off which results in many outcomes depending on the target cell. One outcome is the reduction of chemokine-induced neutrophil migration believed to alleviate the innate immune response to defend against PT-mediated infection. Another outcome is the disruption of the junctions between airway epithelial cells which is linked to the development of edema. This is usually combined with the inhibition of anti-

inflammatory cell signalling resulting in prolonged respiratory inflammation. (Ashok et al. 2020.)

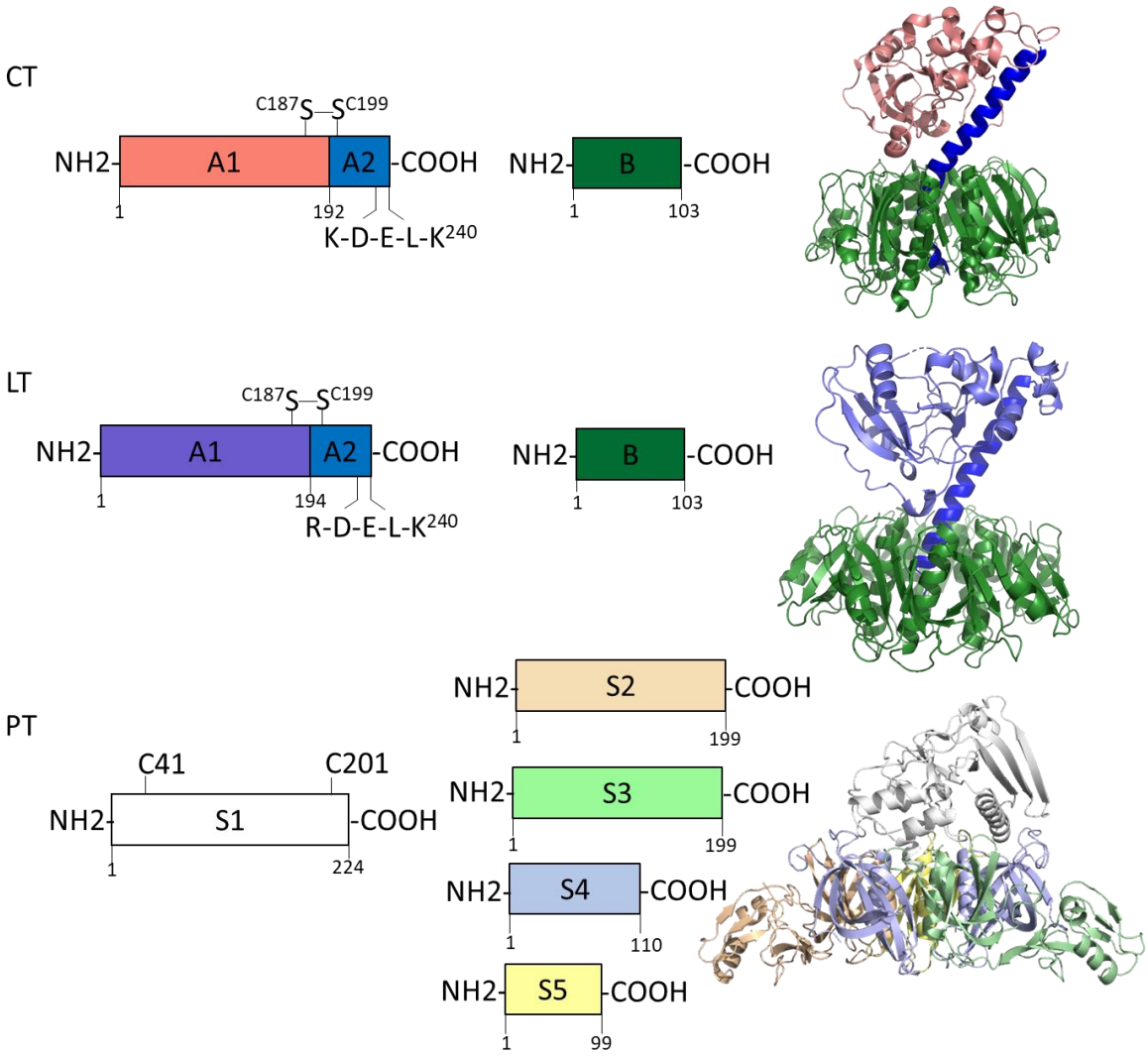

Figure 8. Structural organization of CT, LT and PT and their three-dimensional structures. *The CT-like toxins have an AB_5 structural composition. The receptor binding B_5 subunit is a homopentamer in CT (PDB: 1S5E) and LT (PDB: 1TII) (forest green) and a heteropentamer in PT (PDB: 1PRT) and it comprises one S2 (wheat), S3 (pale green) and S5 (yellow pale) subunits and two S4 (light blue) subunits. CT and LT have a dual-chain subunit consisting of A1 (salmon in CT and slate blue in LT) and A2 (blue) that is connected through a disulphide bridge. The A2 subunit forms a long α-helix through the pentameric B subunit, and it has a C-terminal sequence that is cleaved during translocation inside the cell. PT, on the other hand, has a single chain A subunit called S1 (white). It has an intramolecular disulphide bond between Cys 41 and Cys 201 that is*

reduced before the toxin enters the cytosol. The figure was generated according to Locht and Antoine (1995)*, Heggelund et al.* (2015) *and Masin et al.* (2015).

To summarize, CT, LT and PT take advantage of the host cell's endogenous machinery in order to achieve toxin delivery to the target substrates. After disulphide reduction, which finalizes the activation of the catalytic subunit, the toxin is secreted to the cytosol by hijacking the ERAD-pathway. Once in the cytosol, it interacts with its substrate which are the different G_{α}-subunits of G-proteins.

1.3 Development of toxin-specific inhibitors

One significant outcome of studying and understanding bARTTs or exotoxins in general is the possibility to develop inhibitory molecules against them (Sakari et al. 2022) (Figure 9). These inhibitors are a promising answer to the ever-threating spreading of antibiotic resistance across the globe. Also, the physiological importance of bacterial microbiota places the stress on developing pathogen-specific i.e., toxin-specific pharmaceuticals. Killing or disarming the pathogen does less harm to the host than using antibiotics and killing the whole bacterial microbiota. By specifically targeting the pathogen only, one can reduce the possibility of creating new strains of antibiotic resistant bacteria. There is also a possibility to reducing the usage of antibiotics by using exotoxin targeted derivates in conjunction with antibiotics. (Sakari et al. 2022.)

One clinically significant exotoxin-mediated drug is 2016 the Food and Drug Administration (FDA) approved Bezlotoxumab, a monoclonal antibody designed to target the TcdB toxin of *Clostridium difficile*. Bezlotoxumab is used to treat antibiotic-associated diarrhoea caused by overgrowth of *C. difficile* in the intestines. (Kufel et al. 2017.) It must be noted that TcdB does not belong to the bARTT group of toxins but rather it is a glucosyltransferase (Sakari et al. 2022).

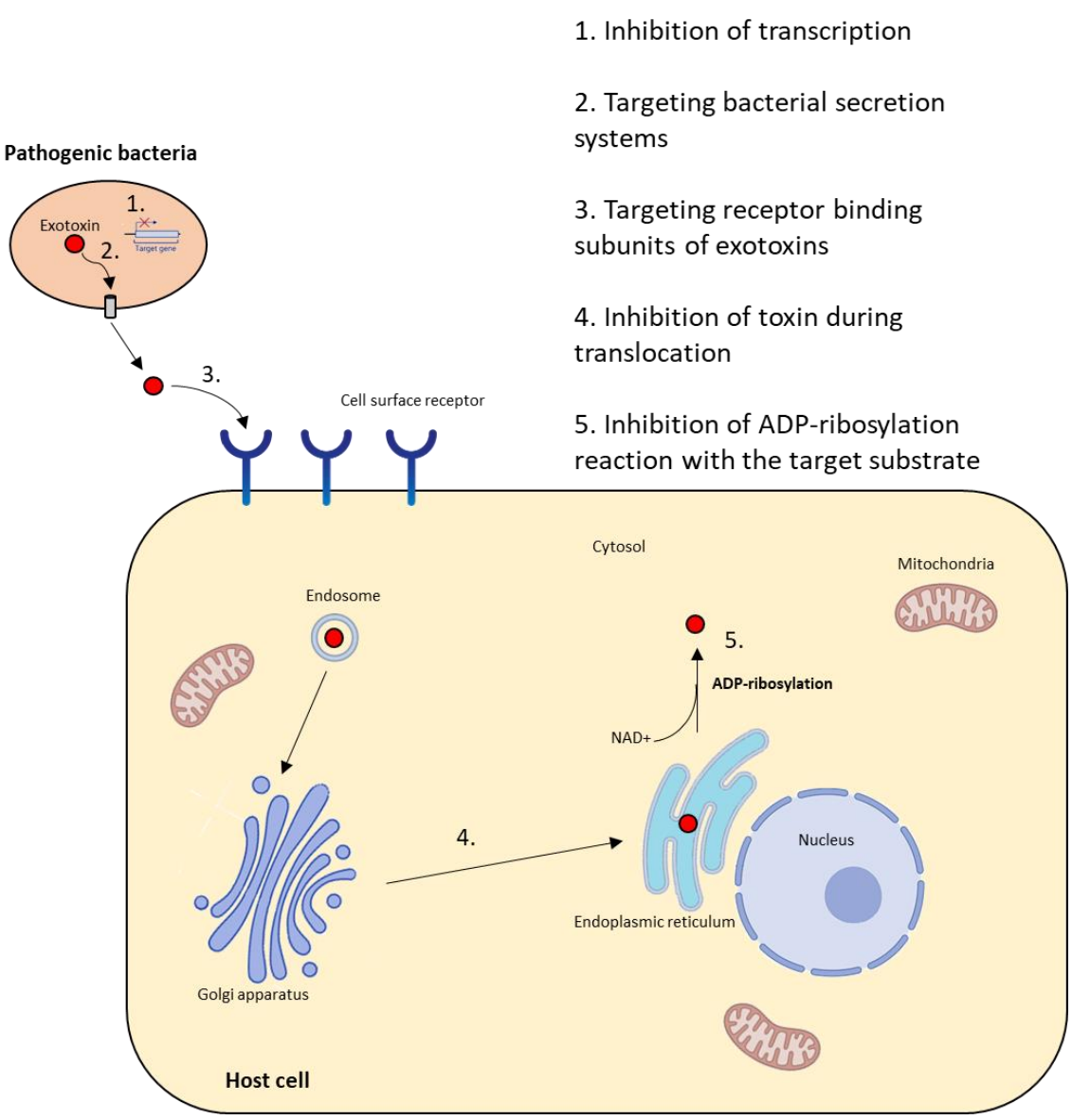

Figure 9. Possible targets for drug development during different stages of toxin induced bacterial infection. *Transcription is a potential druggable target especially in cases where the virulence of the bacteria is caused by one or a few virulence factors. Another option is targeting bacterial secretion systems. This is of course in cases where the bacterial exotoxin is not released when the cell is lysed. When the exotoxin is released, it must find its way to the target cell. This is where knowledge of the B subunit of bARTT comes into play as it could be utilized in vaccine development for example. Once the toxin has infiltrated the host cell, cellular trafficking pathways, from endocytosis through retrograde trafficking could be targeted with small inhibitory molecules. The internalization stage is still poorly understood for therapeutical applications. Theoretically, the development of drugs that target cellular proteins, rather than the toxin itself, may be a better strategy than the use of compounds that*

directly interact with the toxins. The former is likely to have a broader spectrum of action, and resistance may be less likely to develop as quickly. (Harper et al. 2015.) *The last and perhaps more studied step for drug development is the inhibition of the ADP-ribosylation reaction of the target substrate with competitive chemical compounds. This step of drug development is also studied in Pulliainen's lab, the paper by Ashok et al.* (2020) *being one example. The figure was generated with BioRender icons and Microsoft PowerPoint.*

1.4 *Bartonella* species

1.4.1 Overview

Bartonella is a gram-negative pathogenic bacilli bacterium named after its founder Alberto Barton in 1909 (Barton 1909). The *Bartonella* species are facultative intracellular alphaproteobacteria that can be either motile or non-motile. All known *Bartonella* species are pathogenic, and they infect and reside in erythrocytes. (Minnick et al. 2014.) Over 40 *Bartonella* species have been identified to date (Mullins et al. 2017). In addition, currently, more than 100 official, candidate, and subspecies of *Bartonella* have been listed in the List of Prokaryotic Names with Standing in Nomenclature (LPSN) (Parte et al. 2020).

Bartonella are generally transmitted to the host by zoonotic transmission via arthropod vectors such as ticks, lice, fleas, sand flies and biting flies (Koehler et al. 1994; Brouqui et al. 1999). They can also be transmitted through invasive contact such as blood transfusions or through skin lesions that become infected. In addition, there are numerous animal species that act as natural reservoir hosts for *Bartonella*. This includes rodents, ruminants, carnivores, and chiropters i.e., bats. Direct contact with reservoir hosts could be a means for infection although it is highly unlikely to happen. (Krügel et al. 2022.)

1.4.2 Life cycle

Bartonella are slow-growing fastidious aerobic and oxidase-negative species. They are typically cultured in an axenic medium containing hemin at 37 °C with 5 % CO_2, and the media is enriched with rabbit and horse blood. It takes 12 – 14 days for *Bartonella* to

form colonies on blood agar plates but sometimes even up to 45 days to form visible colonies. (Maurin et al. 1994; La Scola and Raoult 1999.) Repeated subculturing reduces colony forming to 3 – 5 days but it also affects the morphology of the colony (La Scola and Raoult 1999). The lack of generic liquid media for *Bartonella* has rendered it difficult to study. However, there is an insect cell media based liquid medium such as Bartonella-Alphaproteobacteria growth medium which is useful in studying some of the known *Bartonella* strains. (Maggi et al. 2005.) Thus, very little of the basic biology of *Bartonella* is known. Information regarding its infection biology for example, has been obtained through studies in animal models such as the *Bartonella tribocorum* rat model (Schülein et al. 2001).

The essential part of a *Bartonella* infection is a long lasting intra-erythrocytic bacteraemia in the reservoir host. The infection typically starts with bacterial colonization of their primary niche, the vascular endothelium. (Schülein et al. 2001; Seubert et al. 2002.) During this time the pathogen evades the hosts innate immune system. This can be due to the inability of Toll-like receptors (TLRs) to recognise the lipopolysaccharide on the outer membrane of *Bartonella*. Some Bartonella evade innate antagonizing proinflammatory factors such as TLR-4. (Zähringer et al. 2004.) Other *Bartonella* species, which have flagella, evade the innate immunity of the host by changing the primary amino acid sequence in their flagellin. This renders them unrecognizable for TLRs which are generally capable of recognising flagella structures. (Scherer et al. 1993.)

When *Bartonella* is released into the bloodstream it can bind to erythrocytes and replicate intracellularly until a certain density is reached. After that the bacterium reaches a static stage where it remains non-replicative for the remaining lifespan of the infected erythrocytes. In this state Bartonella can persist for weeks in circulating blood without causing an infection since infected erythrocytes are indistinguishable from uninfected ones. (Schülein et al. 2001.)

1.4.3 *Bartonella*-induced diseases in humans

Bartonella are known to cause a large range of infections with mild to life threatening symptoms, endocarditis being clinically the most significant disease. Immunocompromised individuals may experience more severe symptoms, and also be

infected with Bartonella species for which humans do not typically act as natural reservoir. 13 of the known *Bartonella* species cause diseases in humans. *Bartonella bacilliforms*, *Bartonella quintana* and *Bartonella henslae* are responsible for most cases of Bartonella-induced diseases. (Jacomo et al. 2002.)

Carrion's disease, otherwise known as bartonellosis is an endemic disease found in western South America and its causative agent is *B. bacilliformis*. It is transmitted by the sandfly *Lutzomyia verrucarum* which is a native species in the high-altitude areas in the Andes. The infection has two phases. The first phase is the acute phase, sometimes called Oroya fever, and its symptoms are fever, the swelling of lymph nodes and severe haemolytic anemia. The chronic phase, also known as the eruptive phase, is the result of the proliferation of the vascular endothelial cells. This causes dermal eruptions that are called verruga peruana. The infection can also be asymptomatic. (Garcia-Quintanilla et al. 2019.)

B. quintana (formely *Rickettsia quintana*) is the causative agent for Trench fever, a disease that was a nuisance to many armies during World War One. The body louse, *Pediculus humanus* is the principal vector for *B. quintana*. Trench fever is characterised by a recycling five-day fever and a headache. (Byam and Lloyd 1920.) The disease disappeared after the Second World War and re-emerged towards the end of the 20th century in individuals with poor hygiene such as in the homeless and in patients suffering from drug addiction. During this time many new *Bartonella*-associated symptoms were found. (Brouqui et al. 1999.) This includes endocarditis which is also associated with *B. henselae* infection and a vasoproliferative disorder called bacillary angiomatosis (BA) that can develop in immunocompromised individuals. The latter disorder is characterised by skin lesions. The infection is progressive and fatal if left untreated. (Gasquet et al. 1998.)

B. henselae is a zoonotic pathogen for which cats act as a natural reservoir. It is transmitted by the cat flea *Ctenocephalides felis* (Chomel et al. 1996; Foil et al. 1998.). Although cats are generally asymptomatic, they can suffer from urological diseases as well as from lymphadenitis, gingivitis, and stomatitis (Ueno et al. 1996). *B. henselae* infection from cats to humans occur by cat scratches or bites or indirectly by the vector. The disease is called Cat-scratch disease, and its symptoms vary, lymphadenitis

being the most common. (Flexman et al. 1995.) As mentioned before, endocarditis and BA can also occur in immunocompromised individuals (Gasquet et al. 1998).

1.4.4 *Bartonella sp. 1-1C*

Small mammals are natural reservoirs for several *Bartonella* species (Inoue et al. 2009). *Bartonella sp. 1-1C* was originally found from the whole blood culture of a wild brown rat *Rattus norvegicus* captured in central Taiwan (Lin et al. 2008). *B. sp. 1-1C* is closely related to *B. rochalimae* which is another *Bartonella* species that was found in 2007 from a traveller in Peru who had received numerous insect bites (Eremeeva et al. 2007). It is not yet known what the vector of *B. sp. 1-1C* is, and whether or not the species is zoonotic (Lin et al. 2008). *B. sp. 1-1C* has been fully draft sequenced (Engel et al. 2011) but no comprehensive studies have been published on it to date excluding phylogenetical studies (Engel et al. 2011; Harms et al. 2017).

2 Aim of the study

Exotoxins are monomeric or polymeric effector proteins that are actively secreted by bacteria or released upon bacterial lysis. They are, in many cases, the main disease-causing virulence factors, such as in cholera infections and whooping cough. The study of exotoxins and their molecular mechanisms provides knowledge that can help in discovering new therapeutic approaches, such as antivirulence drugs, that interfere with the functional pathway of exotoxins during infection. (Sakari et al. 2022.) Previously, the Turku Cellular Microbiology Laboratory has identified *in silico* putative ADP-ribosyltransferase (ART) exotoxins from *Bartonella* bacteria (unpublished data).

The aims of my thesis are to:

1) Express the hexahistidine tagged putative *Bartonella* ARTs in the *E. coli* BL21 (DE3) protein expression strain

2) Purify the proteins with nickel-nitrilotriacetic acid (Ni-NTA) affinity chromatography followed by gel filtration chromatography (size exclusion chromatography, SEC)

3) Characterise the proteins with the following methods:

   - The fold of the proteins is studied with differential scanning fluorometry (DSF)

   - NADase activity of the proteins is studied with endpoint fluorometric homogenous assay

   - Different western blot-based assays having different sensitivities and detection specificities to ADP-ribose are used to study the ART activity of the purified proteins and identify any eukaryotic cell substrate proteins that they may ADP-ribosylate.

3 Materials and methods

3.1 *Bartonella* ART screening

Plasmids containing previously cloned inserts of CtxA Bsch WT, R29A, E135A, CtxA 1-1C WT, E128A/E130A, TRUNC (pET-15b), CtxA Senegalensis (pET-28b), and CtxA Bovis (pMal-c2x) were incubated with the *E. coli* BL21-DE3 protein expression strain (Novagen) for 30 min on ice before transforming the strain with plasmids using heat shock at + 42 °C for 50 s. The transformed bacterial cells were precultured in Luria-Bertani (LB) medium for 1 h at + 37 °C with 220 rpm shaking. After this, cells were plated on LB-agar plates containing either 75 µg/ml of ampicillin or kanamycin and incubated overnight (o/n) at + 37 °C.

The next day colonies were selected and incubated in 5 mL of auto-induction medium (AIM) (Formedium, AIMTB0205) containing 0,8 % glycerol and 100 µg/mL of appropriate antibiotics, either ampicillin or kanamycin. The cells were incubated for 3 h at + 37 °C with 150 rpm shaking before reducing the temperature to room temperature (RT) and incubating for 24 h. The cells were pelleted by centrifuging 4000 x g, 15 min at + 4 °C and resuspended in lysis buffer [100 mM 2-[4-(2-Hydroxyethyl)piperazin-1-yl]ethane-1-sulfonic acid (HEPES), 500 mM NaCl, 10 % glycerol, 2 mM (2S,3S)-1,4-Bis(sulfanyl)butane-2,3-diol (DTT); 0,5 mg/mL lysozyme and 40 µl/mL of 2,2’,2’’,2’’’-(Ethane-1,2-diyldinitrilo)tetraacetic acid (EDTA) free protease inhibitor (Pierce), pH 7,5]. The cells were incubated on ice for 2 h. Lastly the bacterial cells were sonicated on ice in 6 x 15 s + 45 s cycles. A portion of the sonicated cells were stored as total lysates (TOT) in - 80 °C and the other portion was centrifuged 13200 x g, 15 min at + 4 °C. The soluble (SOL) supernatant was collected and stored.

The lysed samples were loaded and run on 12 % sodium dodecyl sulfate–polyacrylamide gel electrophoresis (SDS-PAGE) before blotting them onto nitrocellulose membranes o/n at + 4 °C. The nitrocellulose membranes were washed thrice with 2-Amino-2-(hydroxymethyl)propane-1,3-diol (Tris) buffered saline containing Tween 20 (TBST) (10 mM Tris, 150 mM NaCl; 0,05 % Tween 20, pH 7,5) for 10 min in a rotator at + 4 °C. The membranes were then blocked with 4 % (w/v) bovine serum albumin (BSA) in TBST as mentioned above and probed with 1:1000 rabbit

monoclonal Poly/Mono-ADP ribose (Cat. No.: 83732, Cell Signaling Technology) for 24 – 48 h. The membranes were washed with TBST as mentioned before and incubated with 1:2500 goat antirabbit IgG conjugated horseradish peroxidase (HRP) secondary antibody (sc-2004, Santa Cruz Biotechnology). Incubation was done for 3 h at + 4 °C before washing the membranes thrice with TBST. For anti-His and anti-MBP blots, the membranes were blocked with 5 % milk in TBST. 1:1000 anti-His Tag Purified mouse monoclonal IgG (Cat. No.: MAB050R) was used and it was detected with 1:2500 diluted Goat Anti-Mouse IgG, Human ads-HRP (Cat. No.: 1010-05). 1:1000 anti-MBP HRP-conjugated monoclonal antibody (Cat. No.: E8032L) was used. The membranes were developed with 1:1 Western-BrightECL (Advansta) chemiluminescence reagent and imaged with ImageQuant LAS4000 (GE Healthcare). The images were processed with MultiGauge software (Fuji Photo Film).

3.2 Bioinformatics

The fold of the putative CtxA 1-1C toxin of *Bartonella sp. 1-1C* was predicted with AlphaFold2.0 (Jumper et al. 2021). The protein and ligand structures were prepared using Schrödinger Maestro (Schrödinger Release 2021-2 New York, NY, USA). To obtain the docked conformation of NAD^+, the structure CtxA 1-1C was aligned with the structure of the catalytic cholera toxin A1 subunit co-crystallised with NAD^+ (PDB: 2A5F). Molecular graphics and analyses were performed with UCSF ChimeraX (the Resource for Biocomputing, Visualization, and Informatics at the University of California, San Francisco, USA).

3.3 Large-scale expression and purification of CtxA 1-1C WT, E128A/E130A mutant, and truncated form

Expression plasmids of CtxA 1-1C WT, E128A/E130A (from now on MUT) and TRUNC (N- and C-terminally truncated CtxA) were transformed into the *E. coli* BL21-DE3 strain via heat shock as mentioned before and precultured in Super Optimal broth with Catabolite repression (SOC) medium (2% tryptone; 0,5 % yeast extract, 10 mM NaCl; 2,5 mM KCl, 10 mM $MgCl_2$, 10 mM $MgSO_4$, and 20 mM glucose). The transformed cells were incubated for 1 h at + 37 °C, 220 rpm shaking and centrifuged 2300 x g at RT for 1 min before plating them on LB-agar with 150 µg/mL ampicillin and 1 % glucose. The cells were then incubated at + 37 °C o/n.

The next day, the bacterial lawn from the agar plates was transferred into 1 L of AIM medium with glucose and antibiotics as mentioned before. The cells were cultured at + 37 °C, 150 rpm shaking for 3 h and the temperature was reduced to RT. The bacteria were collected after 24 h by centrifugation and frozen in - 80 °C as pellets. The pellets were resuspended in lysis buffer [100 mM Tris, 500 mM NaCl, 10 % glycerol, 2 mM DTT, 10 mM imidazole; 0,5 mg/mL lysozyme, 250 U benzonase (Millipore, 70664-KUN10)] with protease inhibitors as mentioned before. The resuspended cell pellets were incubated on ice for 30 min and further disrupted with EmulsiFlex-C3 (Avestin). The homogenised lysate was centrifuged 10000 x g, 10 min at + 4 °C and the supernatant was collected and filtered with a 0,45 µm filter. After that, the samples were thoroughly mixed with Ni-NTA agarose beads (Qiagen) and incubated o/n at + 4 °C with rotation.

The following day, the samples were centrifuged 3000 x g 3 min at + 4 °C and loaded to a 5 mL HisTrap HP column (GE Heathcare). The column was washed with eight column volumes of wash buffer with an identical composition to the lysis buffer with the exception of an imidazole concentration of 50 mM. CtxA WT and CtxA MUT were eluted with five column volumes of elution buffer [100 mM Tris, 500 mM NaCl, 10 % glycerol; 0,5 mM 3,3',3''-Phosphanetriyltripropanoic acid (TCEP), 1 % NP-40, 500 mM imidazole, pH 7,0]. CtxA TRUNC was eluted with the same buffer composition except no NP-40 was added.

The proteins (CtxA WT, MUT and TRUNC) were further purified with size exclusion chromatography (SEC) using a HiPrep Sephacryl 16/60 S-400 HR column (Cytiva). The column was equilibrated with three column volumes of elution buffer having the same composition as the Ni-NTA buffer except no imidazole was added. The samples were run at 0,75 mL/min flow rate. The peak fractions were collected, and their quality assessed with SDS-PAGE and PAGEBlue staining. After that, fractions were pooled and concentrated using a 10 kDa cutoff concentrator (Thermo Scientific). Concentrations for each pooled protein were measured with Bradford assay (Bio-Rad) and proteins were stored in - 80 °C.

3.4 Differential scanning fluorometry analysis

10 µM of SEC purified CtxA proteins were incubated with 5 x SYPRO orange in MQ (Invitrogen, Cat. No.: S6650) on a 96 PCR well plate for 10 min. The samples were heated from 20 °C to 95 °C with 0,5 °C increments (1 min/ 1 °C) and measured as triplicates. The experiment was run on a Bio-Rad C1000 Thermal Cycler with a CFX96 Real-Time PCR detection system. The melting temperature (T_m) values were determined by using the CFX96 Real-Time PCR detection system software (Bio-Rad) and the graphs were displayed with Excel.

3.5 *In vitro* NAD^+ consumption assay

30 µM of Ni-NTA purified CtxA 1-1C WT, MUT, TRUNC and 0 – 50 µM of β-NAD^+ (Sigma) was titrated on a black 96 chimney well microplate (Greiner Bio-One) in the presence of 50 mM sodium phosphate buffer (pH 7,0) and incubated for 2 h at RT with 300 rpm shaking. 20 % acetophenone in ethanol and 2 M KOH were added and incubated 10 min at RT. After that 100 % formic acid was added and the plate was incubated in RT for 20 min. The plate was read with Hidex Sense with excitation and emission wavelengths set at 355 and 450 nm, respectively.

3.6 HEK293T and RAW264.7 cell lines for substrate preparation

Human embryonic kidney (HEK293T) and murine macrophage (RAW264.7) cell lines were maintained in Dulbecco's Modified Eagle's Medium (DMEM) (Lonza) supplemented with 6 mM L-glutamine and 10 % Foetal Bovine Serum (FBS) at + 37 °C with 5 % CO_2. For preparing the soluble cell lysates, 60 – 80 % confluent HEK293T and RAW264.7 cells in T75 flasks were washed twice with Phosphine Buffered Saline (PBS) and detached with Trypsin-EDTA. The cells were collected by scraping and centrifuged 500 x g, at RT for 5 min. The cell pellet was resuspended in Radioimmunoprecipitation assay buffer (RIPA) [50 mM Tris, 200 mM NaCl, 1 % (w/v) Sodium deoxycholate; 0,1 % SDS, 1 mM EDTA with 40 µl/mL of Pierce Protease and Phosphatase inhibitor (Thermo Scientific) and 25 U of benzonase, pH 8,0] and incubated for 1 h on ice. The total cell lysate was centrifuged 21130 x g, at + 4 °C for 10 min and the soluble fraction (soluble cell lysate) was collected and stored in - 80 °C.

3.7 *In vitro* ADP-ribosylation assay

3.7.1 ADP-ribosylation reaction setup

Reactions with a total volume of 50 µl containing SEC or Ni-NTA purified proteins and 10 µM of either biotinylated NAD^+ (Trevigen) or 10 µM of β-NAD^+ and either with the presence or absence of soluble lysates of HEK293T and RAW264.7 were prepared. The ADP-ribosylation reactions were carried out in RT for 2 h at 400 rpm shaking. The reactions were stopped by adding Laemmli loading dye (65 mM Tris, 2 % SDS, 25 % glycerol; 0,01 % bromophenol blue, pH 6,8) with 5 % β-mercapthoethanol added before usage and heating the samples for 10 min at 95 °C. The reaction samples were stored in - 20 °C or cleared by centrifugation 11000 x g for 1 min and loaded for gel electrophoresis.

3.7.2 Western blot read-out of ADP-ribosylation reactions

The samples were loaded and run on 12 % SDS-PAGE gels before blotting them onto nitrocellulose membranes o/n at + 4 °C. The nitrocellulose membranes were washed thrice with TBST for 10 min in a rotator at + 4 °C. For biotinylated NAD^+ reactions, the membranes were blocked with 1 % (w/v) casein blocking buffer (Biorad) in TBST for 3 h. After that the membranes were incubated with a solution of streptavidin-HRP 1:5000 (GE Healthcare) in 1 % casein blocking buffer for 3 h at + 4 °C and washed thrice with TBST. For ordinary NAD^+ reactions, the membranes were blocked with 4 % w/v BSA in TBST and probed with 1:1000 rabbit monoclonal Poly/Mono-ADP ribose antibody for 24 – 48 h. The membranes were washed as mentioned before and incubated with 1:2500 goat antirabbit IgG conjugated HRP secondary antibody. The membranes were incubated for 3 h at + 4 °C before washing thrice with TBST. The anti-His blots were done as mentioned before. The membranes were developed with 1:1 Western-BrightECL chemiluminescence reagent and imaged with ImageQuant LAS4000. The images were processed with MultiGauge software.

4 Results

4.1 *Bartonella sp. 1-1C* has the most active and soluble protein

Screening of enzymatically active ADP-ribosyltransferases from bacterial lysates without further purifying them is one way to evaluate potential candidate enzymes for further studies. A small-scale expression of 5 mL was prepared for plasmid constructs containing candidate toxin genes from *Bartonella* species. In my case, I was interested in the proteins with the most vibrant automodification activity. According to the anti-MAR/PAR blot of the total cell lysate (TOT) (Figure 10 A) the Wildtype (WT) CtxA of *Bartonella sp. 1-1C* is the most enzymatically active toxin compared to the other three screened toxins of *Bartonella* species i.e., *B. schoenbuchensis* (Bsch), *B. senegalensis*, and *B. bovis*. However, only CtxA of *B. sp. 1-1C* was active in the soluble cell lysate (SOL) (Figure 10 B). All the other proteins are pelleted into the insoluble fraction. Overall, the transformation was successful according to the anti-His blot of the TOT blot as clear 14 – 35 kDa bands can be seen for all the His-tagged proteins. The MBP-tagged CtxA bovis is also successfully expressed as the protein can be seen on the SOL blot of the anti-MBP blot albeit not in the TOT blot (Figure 10).

The His-tagged CtxA Bsch and 1-1C both have auto ADP-ribosylation activity that will not be seen once the point mutations (R29A and E135A in Bsch, E128A and E130A in 1-1C [from now on CtxA 1-1C MUT]) take place. The truncated 14 kDa CtxA of 1-1C (CtxA TRUNC) is active in the total lysate but loses its activity in the soluble lysate (Figure 10 B). The solubility of CtxA TRUNC also decreases. The CtxA of *B. senegalensis* and the maltose-binding protein (MBP) tagged CtxA of *B. bovis* posess no auto-ADP-ribosylation activity as no clear band of 35 kDa or 50 kDa bovis can be seen in the total lysate of the anti-MAR/PAR western blot (Figure 10 A). Although, a 25 kDa high intensity band can be seen in the total lysate of CtxA bovis which is distinctive of that in the empty pMal-c2x control. Interestingly, I failed to detect CtxA bovis on the anti-MBP western blot of the total lysate, but it was visible on the soluble lysate (Figure 10 B).

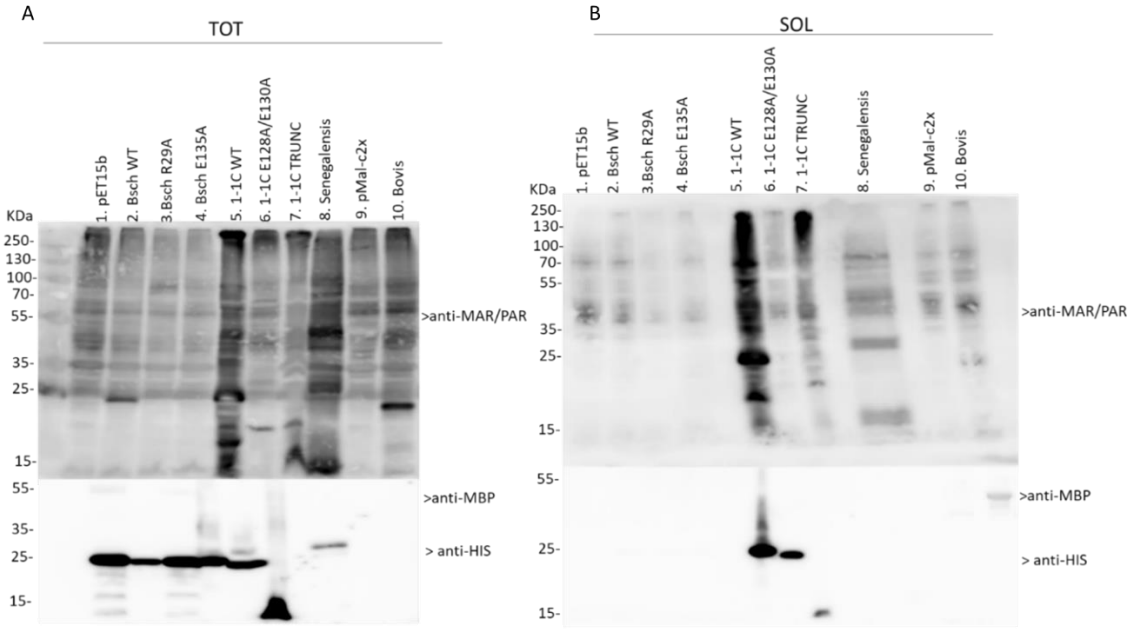

Figure 10. ***CtxA auto-ADP-ribosylation activity screening of Bartonella species B. schoenbuchensis (Bsch), B. sp.1-1C, B. senegalensis and B. bovis with anti-MAR/PAR western blot from lysed E. coli BL21 DE3 cells. (A)*** *Total lysate (TOT) indicates that the cells were resuspended in lysis buffer and sonicated before running them on an SDS-PAGE gel and transferring onto nitrocellulose membrane. 1. pET15b is a control reaction, an empty plasmid with no insert. 9. pMal-c2x is an empty plasmid containing the maltose-binding protein (MBP) solubility tag. It is used as a control for the MBP-tagged 10. CtxA bovis. 2. Bsch WT, 3. Bsch R29A, 4. Bsch E135A, 5. 1-1C WT, 6. 1-1C E128A/E130A (MUT), 7. 1-1C TRUNC were all expressed in pET15b plasmid. 8. Senegalensis was expressed in a pET28b plasmid.* ***(B)*** *Soluble lysate (SOL) indicates that a fraction of the samples was centrifuged to pellet the insoluble material. kDa on the left-hand side of the blots indicate the molecular weight of the bands in kilodaltons.*

4.2 The structure of CtxA 1-1C was generated with AlphaFold

Since no experimental data is available on the structure of CtxA 1-1C of *Bartonella*, AlphaFold was used to predict the structure of the protein. AlphaFold is an artificial intelligence software which is used to predict the structures of proteins based on their amino acid sequence. The software successfully generated a tertiary structure for CtxA 1-1C (Figure 11 A). It predicted that CtxA has two large and two small α-helices with an anti-parallel β-sheet and three loop-regions (Figure 11 B). The catalytic site was

recognised as having an RSE motif which is a characteristic of bARTTs belonging to the CT-like group. The catalytic sites were recognised as Arg27, Ser81, Glu128 and Glu130 (the Glu residues make up the EXE-motif). NAD^+ was docked and aligned to the catalytic site of the protein (Figure 11 C-D) to show a possible way of NAD^+ binding for ADP-ribosylation reaction catalysis. Superimposing the CTA1 catalytic site with the predicted fold of CtxA showed no mismatches.

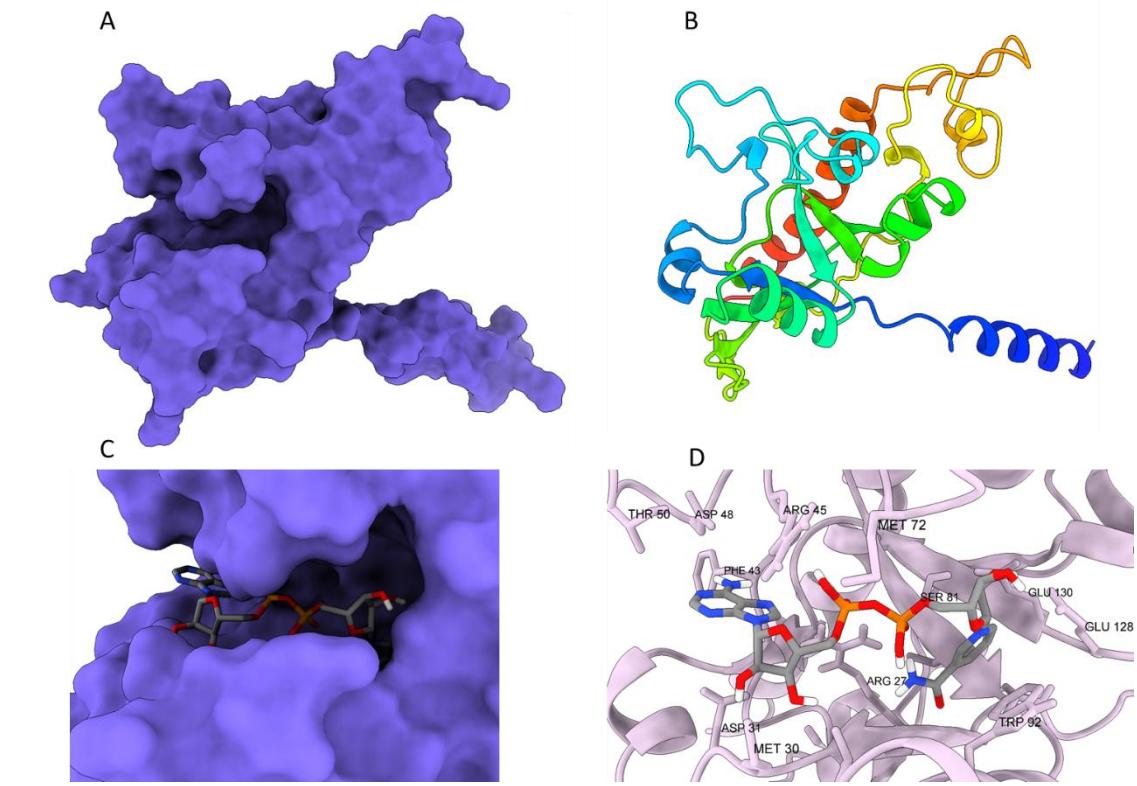

Figure 11. Structural model of CtxA 1-1C. (A) *Surface representation of CtxA 1-1C generated with AlphaFold.* ***(B)*** *The tertiary structure of CtxA 1-1C. The blue α-helix could represent the A2 subunit that is also seen in CT and LT. This subunit acts as a scaffold between the A and B subunits.* ***(C)*** *The possible binding of NAD^+ to the active site of CtxA 1-1C is derived from superimposing the predicted fold of CtxA 1-1C with cholera toxin A1 (CTA1) subunit co-crystallised with NAD^+ (PDB: 2A5F).* ***(D)*** *A closer look of how NAD^+ is bound to the active site. The core of the catalytic site is composed of Arg27, Ser81, Glu128 and Glu130 residues. The ligand docking was done with Schrödinger Maestro and molecular graphics displayed with UCSF ChimeraX. The figures were generated with the help of Dr. Rajendra Bhadane.*

4.3 Large-scale purification of CtxA-1-1C WT, MUT, and TRUNC is successful

CtxA 1-1C WT, MUT and TRUNC were transformed and expressed in a large-scale purification experiment for further studies. In my study, I used autoinduction medium (AIM) instead of Isopropyl β-D-1-thiogalactopyranoside (IPTG) induction to express the proteins. Doing so minimizes the chance that my proteins aggregate because of a strong and sudden activation of the lac promoter. I also used it for more practical reasons; to ensure that my protein is expressed slowly over time. This in turn ensures that the cells can withstand the expressed proteins since they are all potential toxins, consuming metabolically important NAD^+, that could be harmful for the bacterial cells. By using AIM, the bacteria are allowed to consume all glucose naturally with no need for monitoring OD_{600}. After that they switch to the induction sugar, lactose in my case. I also added 0,8 % glycerol to the media for further enhancing the growth of the culture and as a secondary carbon source.

After the cells have grown, been subjected to centrifugation and lysis, their expressed proteins are purified from the crude bacterial lysate with immobilized metal affinity chromatography (IMAC). IMAC is a separation technique that utilizes chelates, such as transition-metal ions immobilized on a resin matrix that capture the protein of interest. In order to achieve this, a histidine (His) tag is required as a part of the recombinant protein structure. The lysate is loaded and washed with a buffer containing 50 mM of imidazole to interfere with the weak binding of other proteins and to elute proteins that bind weakly with the metal chelate. The His-tagged protein is then eluted by increasing the imidazole concentration to 500 mM. The high imidazole concentration competes for binding positions with the protein of interest, eventually replacing it.

The N-terminally His-tagged CtxA WT was successfully purified with nickel-nitriloacetic acid (Ni-NTA) chromatography. The eluted protein has impurities (Figure 12 A) but the main 25 kDa band is clearly visible and verified with the anti-His blot (Figure 12 B). The total protein yield from the Ni-NTA eluates is 42,8 ± 0,3 mg.

CtxA 1-1C MUT was successfully captured with Ni-NTA agarose beads and eluted with 500 mM imidazole. The eluates are less impure than those of CtxA 1-1C WT (Figure 13

A), but the protein yield is also lower with 19,8 ± 0,7 mg. The 25 kDa band is clear on the anti-His blot, and it is visible in the bacterial lysate (Figure 13 B).

CtxA TRUNC was successfully purified but proved to be the most impure out of the studied proteins (Figure 14 A). The 14 kDa product cannot be clearly identified from the PAGEBlue staining but it was verified with the anti-His blot of the eluates. There is no 14 kDa band for E1 on the PAGEBlue stained gel but it is seen on the anti-His blot with high intensity. Interestingly, there was a considerable amount of protein lost after centrifugation and filtration as well as in the flow-through as clear 14 kDa bands can be seen on the anti-His blot (Figure 14 B). The protein yield is 20,1 ± 1,2 mg.

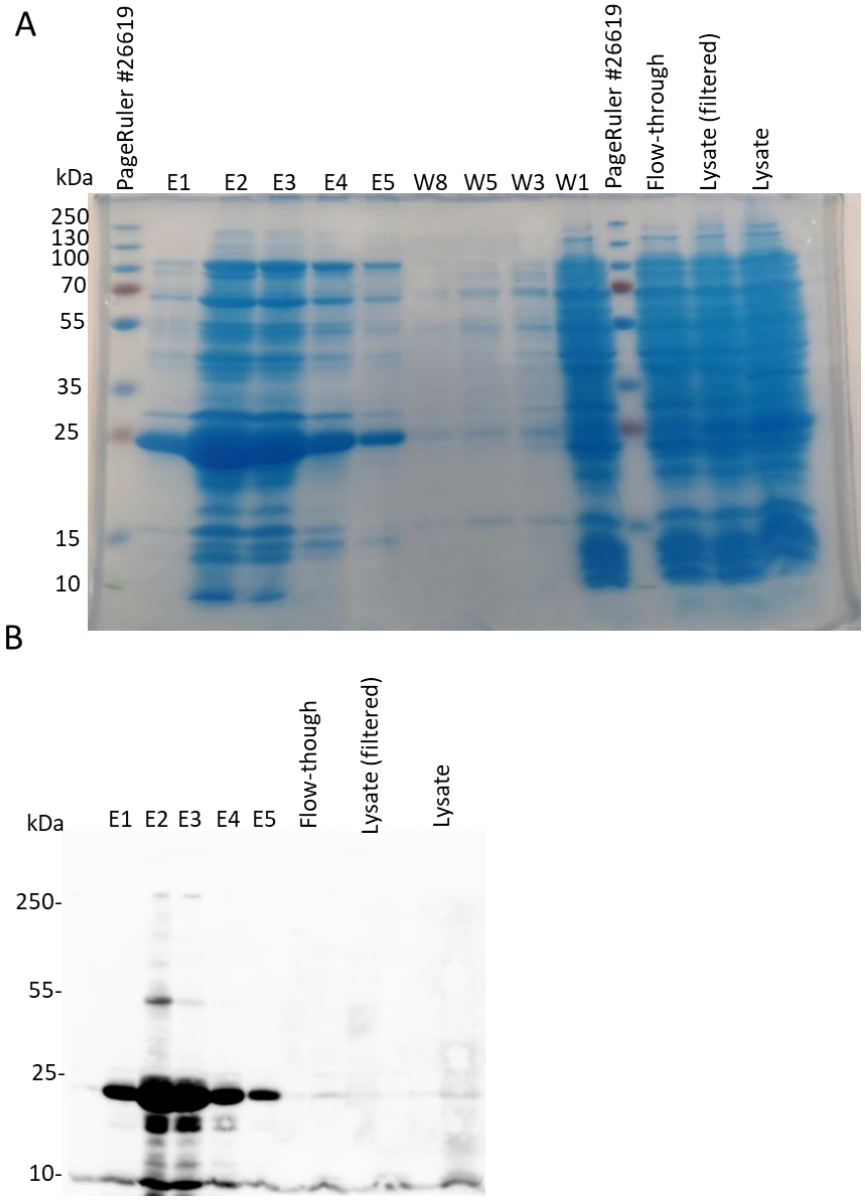

Figure 12. ***CtxA WT***

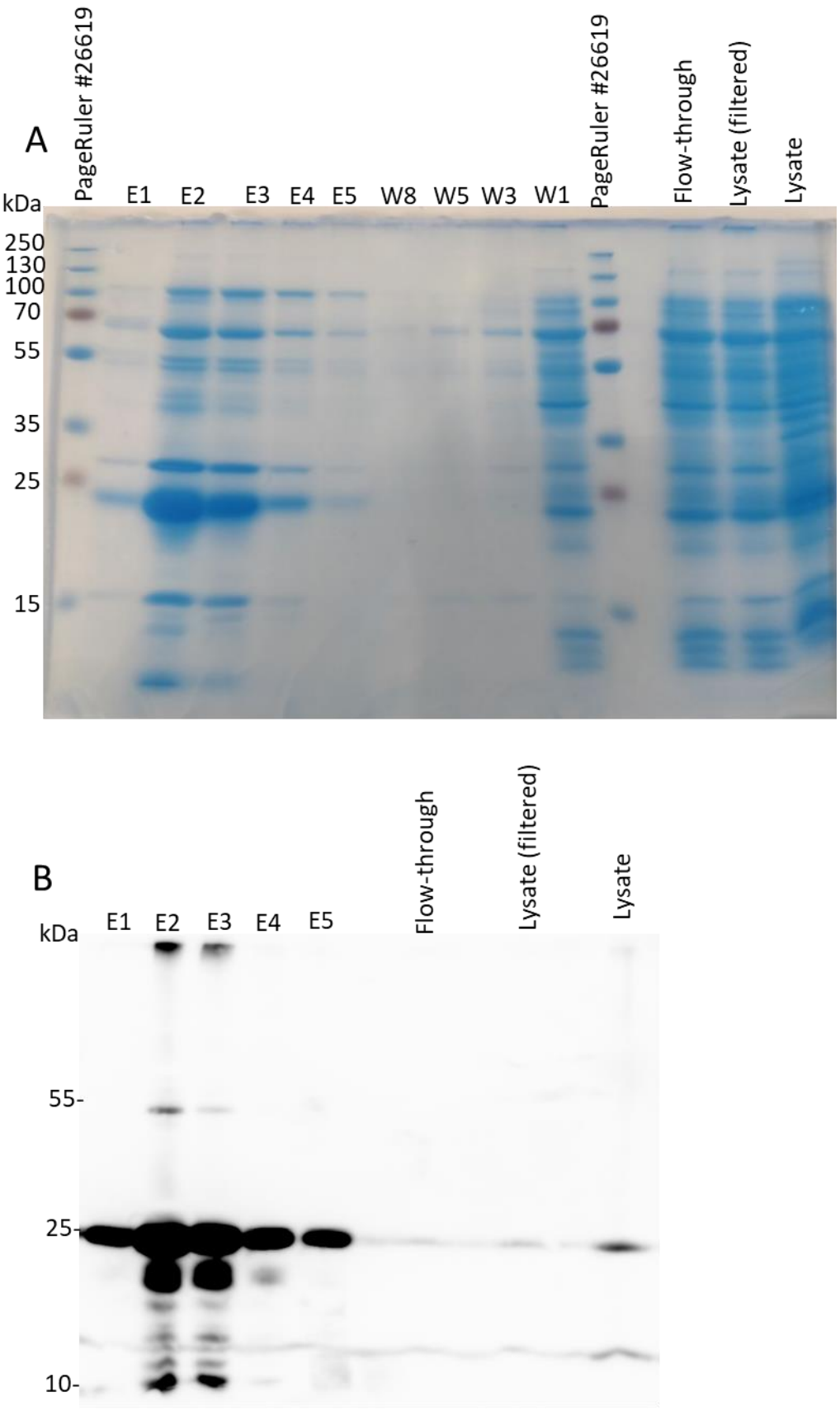

Figure 13. ***CtxA MUT***

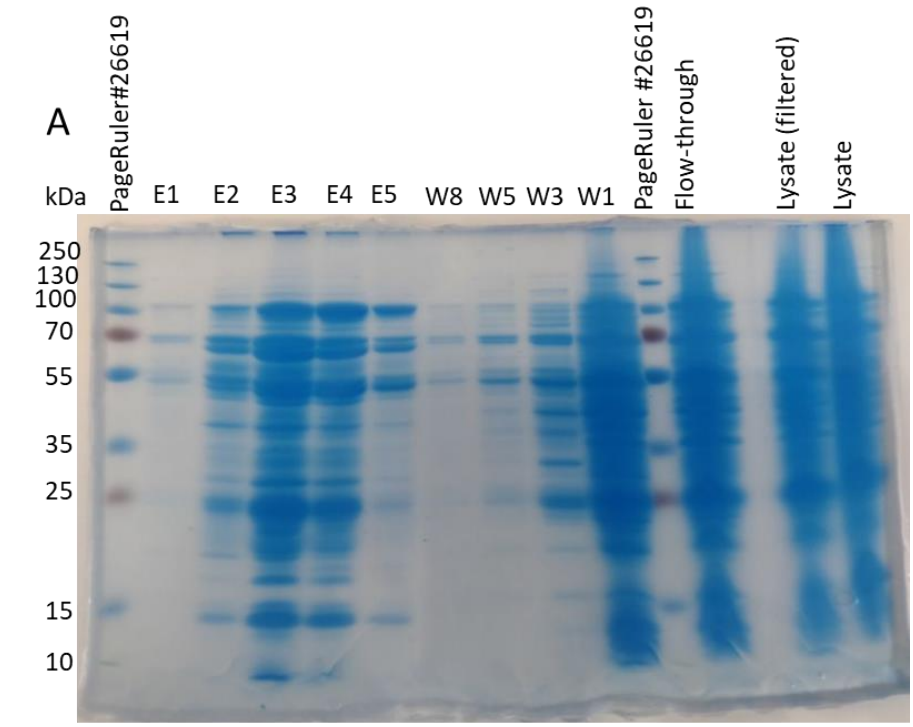

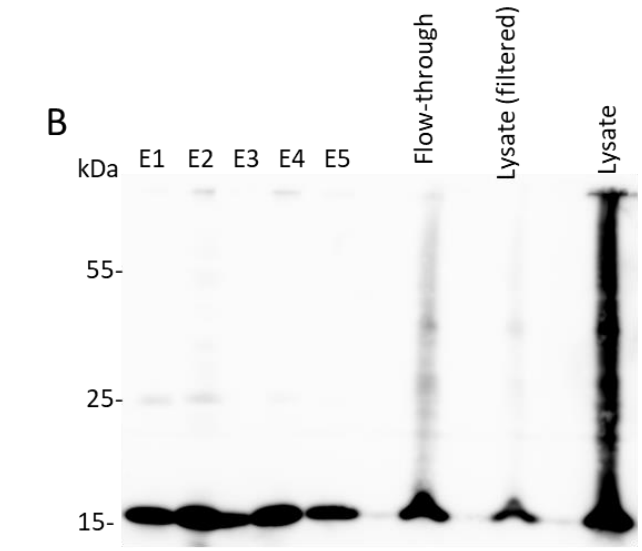

.

Figure 14. ***CtxA TRUNC***

Figures 12 – 14. ***Evaluation of Ni-NTA purification steps for CtxA 1-1C WT, MUT and TRUNC. (A)*** *PAGEBlue staining of 12 % SDS-PAGE gel. E stands for Eluate and W for Wash. Lysate is a sample taken immediately after homogenisation with emulsiflex. Lysate (filtered) is a centrifuge cleared and 0,45 µm filtered sample. Flow-through is the sample after the filtered lysate was loaded and drained through the column. Eight washes were done with 50 mM imidazole concentration and washes 1, 3, 5 and 8 were evaluated. The captured His-tagged protein was eluted five times with 500 mM*

imidazole. ***(B)*** *The samples were verified with an anti-His western blot where 14 – 25 kDa bands can be seen.*

4.4 SEC-purification of CtxA 1-1C WT and MUT is successful

Size exclusion chromatography (SEC) is a form of partition chromatography where molecules of interest are partitioned between a mobile phase and a stationary phase as a function of their relative sizes. The mobile phase is a buffer that carries the sample through the stationary phase which comprises a porous bead matrix packed in a column. The column has two volumes, the external volume, and the internal volume. The external volume (the liquid between the beads) is referred to as the void volume V_0. The sum of external and internal volumes is called total volume V_t. During a SEC run, molecules larger than the pores of the stationary phase will be excluded from the internal volume within the beads. Therefore, the molecules migrate rapidly through the column, emerging at V_0, while molecules both smaller than the matrix pores, as well as those intermediate in size, will equilibrate with both the external and internal liquid volumes, causing them to migrate much more slowly and emerge at an elution volume (V_e) greater than V_0. Thus, the molecules are eluted in order of decreasing molecular size. V_e of a particular molecule depends on the fraction of the stationary phase available to it for diffusion. (Walls and Walker 2017.)

CtxA 1-1C was further subjected to SEC for a purer product. Previously CtxA 1-1C WT was purified with an S-200 column which has a fractionation range of 5 – 250 kDa. It would have been a more suitable and logical option for a protein that has a molecular weight of 25 kDa. However, the protein eluted in V_0 which is uncharacteristic for a properly folded globular protein. Therefore, CtxA WT, MUT and TRUNC were purified with an S-400 column which has a fractionation range of 10 – 2000 kDa. CtxA 1-1C WT was successfully purified with SEC. The protein eluted 17 mL after reaching the V_0 volume of 43 mL of the used HiPrep Sephacryl 16/60 S-400 HR column (V_e = 60 mL) The maximum peak was at 88 mL when the absorbance was A_{280} = 20 mAU (Figure 15). The eluted fractions of 25 kDa were verified with a 12 % PAGEBlue stained SDS-PAGE gel (Figure 16) and they were free from interacting impurities. The smaller peak seen after reaching the V_t volume of 120 mL did not contain any proteins.

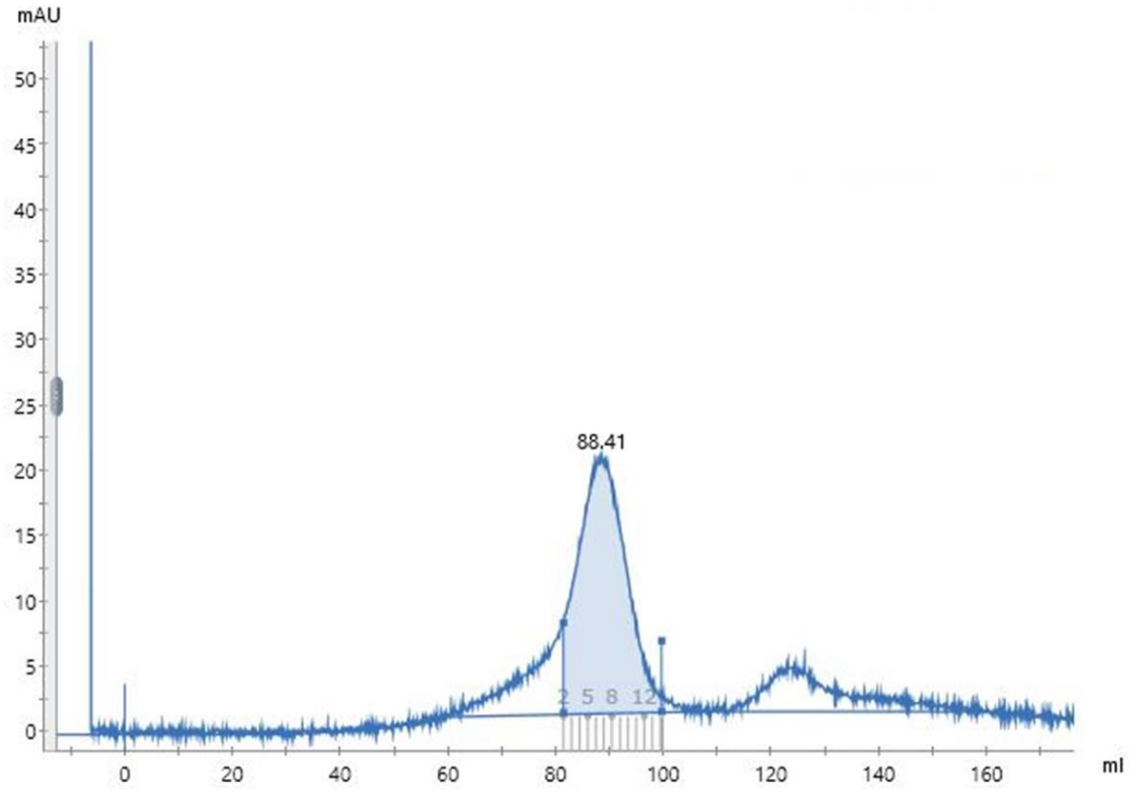

Figure 15. Chromatogram of size-exclusion chromatography (SEC) purified CtxA 1-1C WT. *The protein was purified with ÄktaPure using a HiPrep Sephacryl 16/60 S-400 HR column. The y-axis indicates milli absorbance units (mAU) at 280 nm whereas the x-axis indicates how much buffer has run through the column. The main peak of CtxA 1-1C WT started at 60 ml and was fully eluted at 100 ml. The numbers from 2 – 12 indicate the eluates collected.*

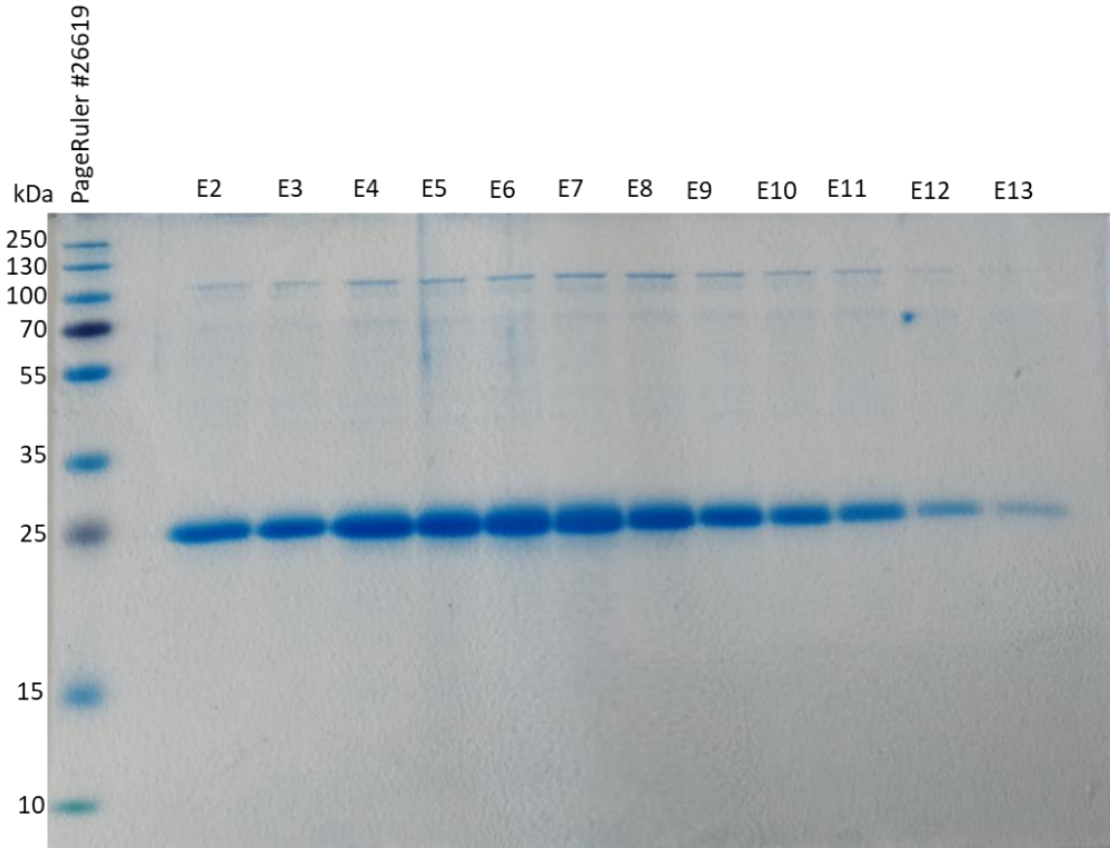

Figure 16. SEC purified eluates of CtxA 1-1C WT on 12 % SDS-PAGE gel. *The eluates are clear of major impurities, and the 25 kDa monomer main product is shown.*

CtxA MUT had the same elution profile as CtxA WT with the protein starting to elute at V_e= 2560 mL while the sample was injected at V= 2500 mL. The maximum peak reached 17 mAU (Figure 17) at 2588 mL. Despite having the same elution profile as CtxA WT, CtxA MUT had a broader main peak. Notwithstanding, the main 25 kDa product was verified with an SDS-PAGE gel (Figure 18). CtxA TRUNC was also purified with SEC. Despite having sharp peaks, the eluates were impure, and no 14 kDa product was seen on the SDS-PAGE gel (data not shown). Hence, no further studies were done with SEC purified CtxA TRUNC.

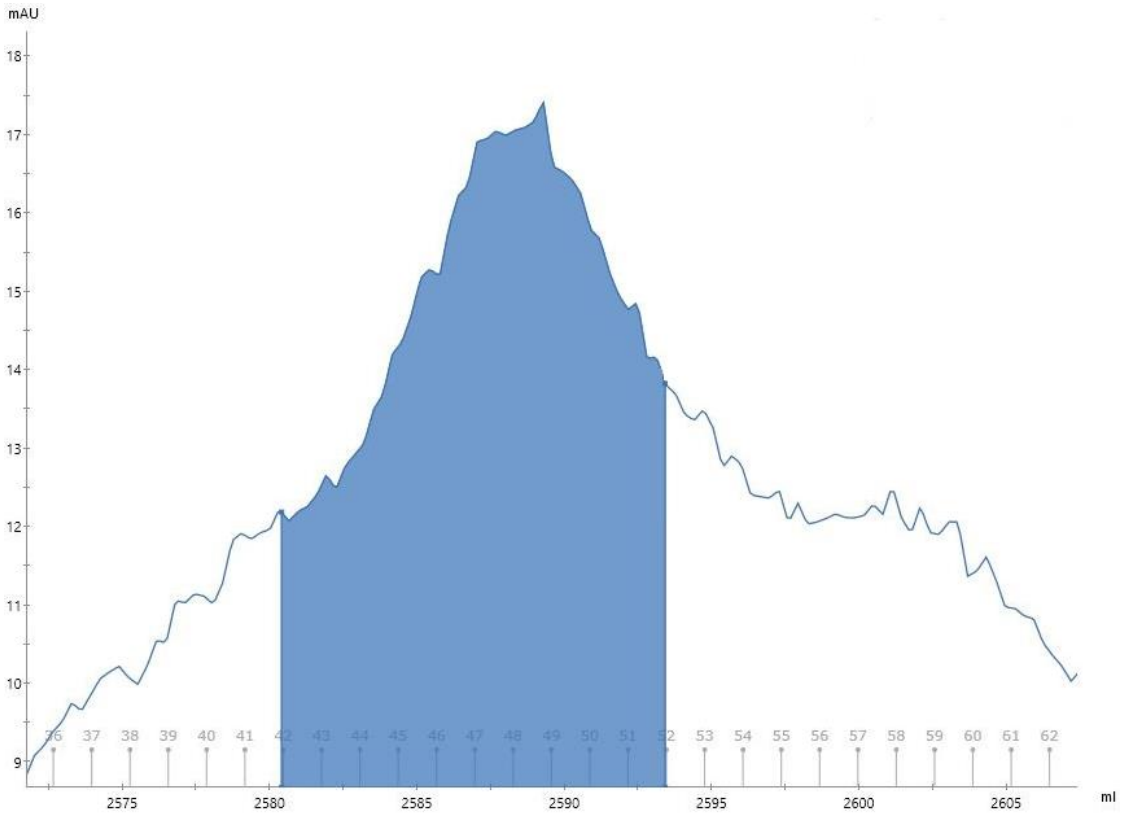

Figure 17. Chromatogram of SEC purified CtxA MUT. *The chromatogram is zoomed on the main peak.*

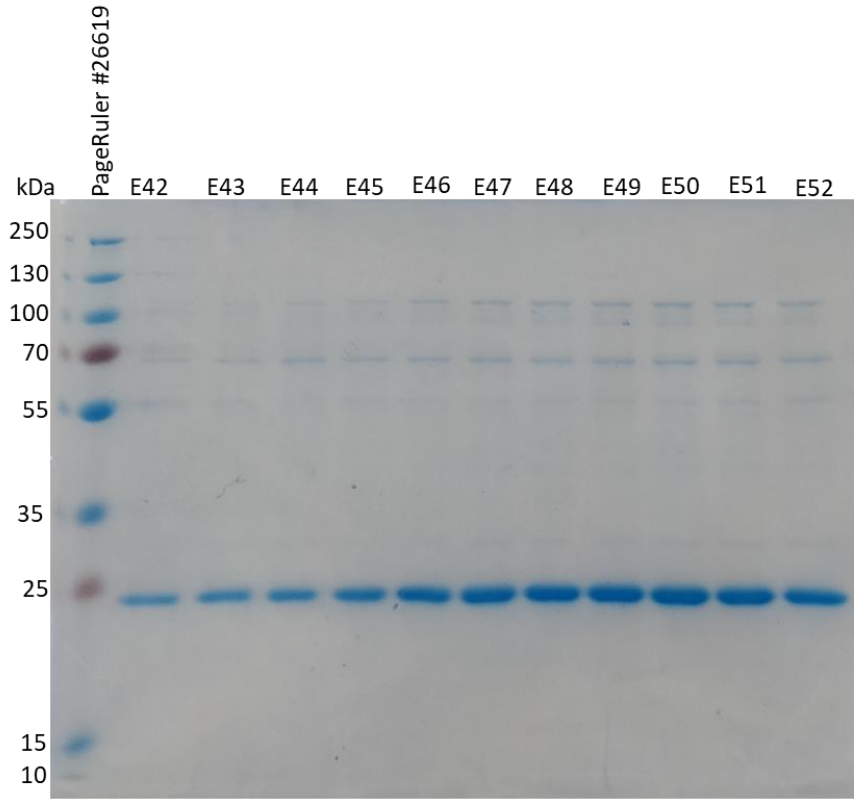

Figure 18. PAGEBlue staining of the collected SEC-eluates from the main peak of CtxA MUT on a 12 % SDS-PAGE gel. *The 25 kDa product is shown.*

4.5 DSF indicates that neither CtxA 1-1C WT nor MUT is properly folded

The first step of evaluating the purified proteins was to study their fold with differential scanning fluorometry (DSF). This is done as a simple 96-PCR plate reaction with the SYPRO Orange dye, that interacts with hydrophobic residues of the amino acids as the protein is denaturated. The reaction releases a fluorescent signal that is measured while the sample is heated. Only SEC purified proteins were used in this experiment as it was postulated that Ni-NTA purified proteins would not be pure enough to give a realistic interpretation of their fold. Hence, only CtxA 1-1C WT and MUT were studied as I failed to SEC purify CtxA 1-1C TRUNC. CtxA 1-1C WT and MUT both had very high initial fluorescence values compared to the positive control PtxS1 which is the A subunit of PT (Figure 19). In a properly folded protein such as PtxS1, the fluorescence values gradually start to increase until the melting temperature (T_m) is reached. When T_m is reached the hydrophobic amino acid residues are exposed due to protein unfolding and the dye binds to them. The T_m of PtxS1 is 53,5 ± 0 °C. The T_m of CtxA 1-1C WT was 81,0 ± 1,1 °C. The T_m of CtxA 1-1C MUT was 87,2 ± 4,5 °C. The program calculated T_m values for the CtxA buffer ranging between 78 °C – 84 °C.

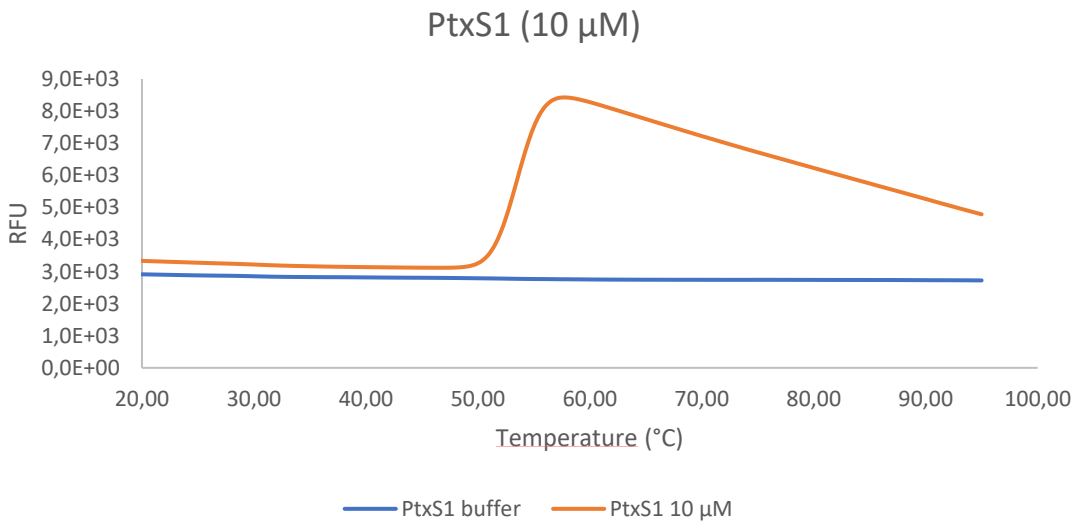

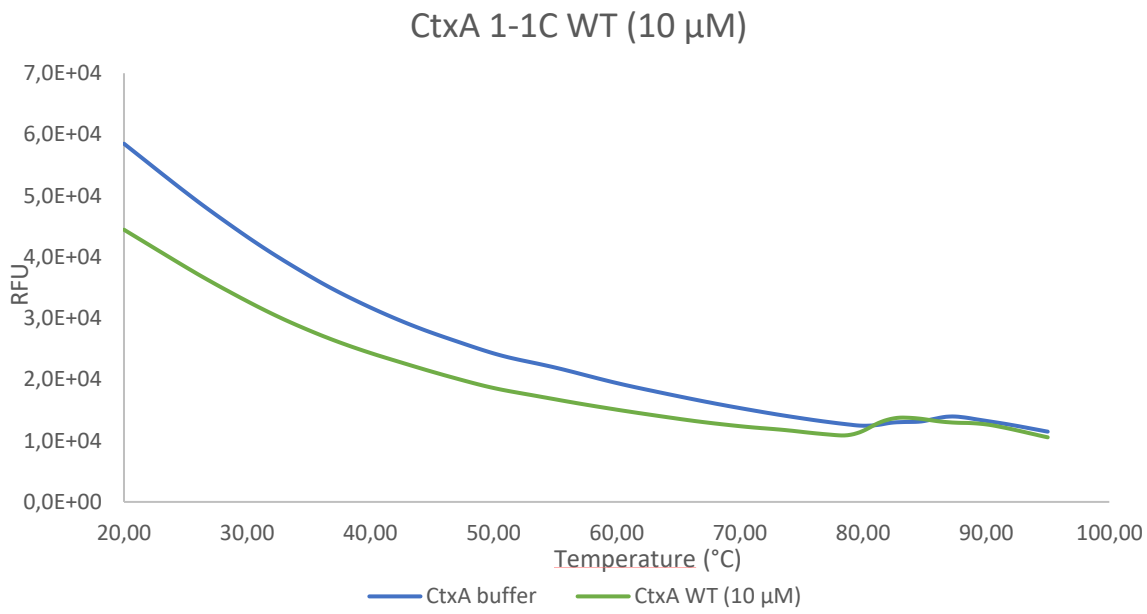

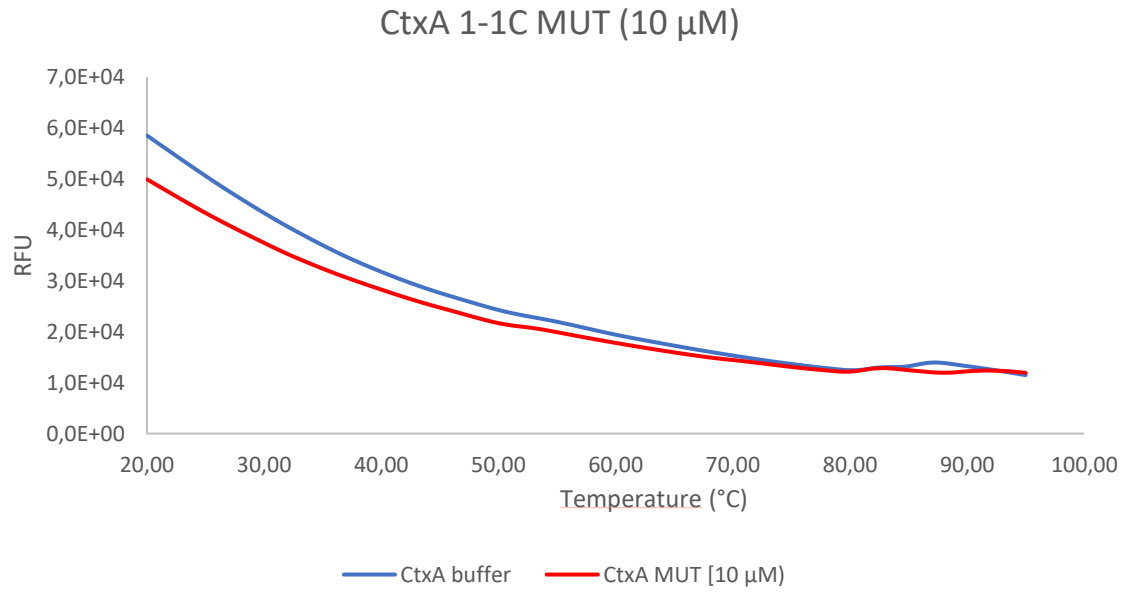

***Figure 19. DSF melting curves of CtxA 1-1C WT and MUT**. SEC purified PtxS1 is used as a positive control to indicate how a well-folded globular protein would behave. The buffer response to the assay is shown. Ideally the buffer should give a flat response indicating that the dye does not interact with the buffer components. However, in the case of CtxA 1-1C WT and MUT, which both have the same buffer composition, the buffer response is initially very high, indicating that the SYPRO orange dye interacts with the buffer components, giving a high background signal. The fluorescence values are displayed as relative fluorescence units (RFU).*

4.6 CtxA 1-1C does not hydrolyse NAD^+

As ADP-ribosylation is a NAD^+-dependent reaction, I wanted to know whether my proteins possess NAD^+ hydrolase activity. It is known that PtxS1 has NAD^+ hydrolase activity even without the addition of its target substrate (Masin et al. 2015). The experiment was done on a 96 well plate using an end-point measurement of NAD^+. The leftover NAD^+ from the reaction is chemically converted to a detectable fluorophore via reaction with 20 % acetophenone and formic acid. The fluorophore called 3-phenyl-2,7-naphthyridin-1(7H)-one has excitation and emission maximums of 372 nm and 444 nm respectively (Figure 20).

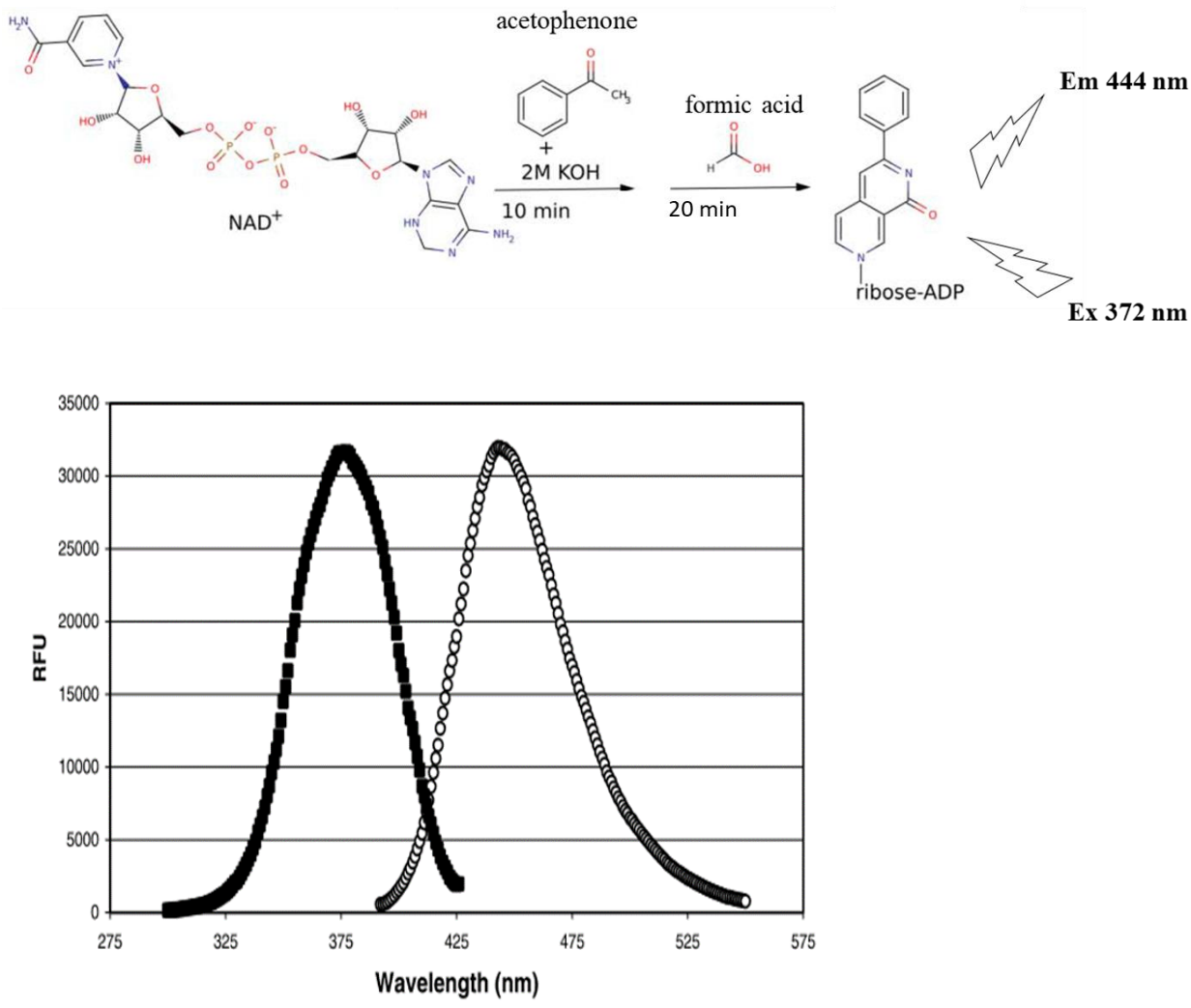

Figure 20. The chemical reaction and the excitation and emission spectra of chemically synthetised NAD^+ analog 3-phenyl-2,7-naphthyridin-1(7H)-one. *The excitation maximum (black curve) is at 372 nm and emission maximum (white curve) at 444 nm.* (Putt and Hergenrother 2004)

The NADase consumption was measured at three NAD^+ concentrations: 0, 5 and 50 µM. 30 µM of Ni-NTA purified CtxA 1-1C WT, MUT, and TRUNC was used whereas 5 µM of PtxS1 acted as a positive control. As can be seen, only PtxS1 is able to hydrolyse both NAD^+ concentrations effectively, the RFU values decreasing to $3,0 \times 10^4$ and $3,6 \times 10^5$ (red and green columns of PtxS1 5 µM) whereas no effect can be seen with CtxA as the RFU values range between $2,0 \times 10^5$ with 5 µM NAD^+ and $1,3 \times 10^6$ with 50 µM NAD^+ (Figure 21). Interestingly, all the fluorescent values of CtxA (WT, MUT and TRUNC) are higher than those of their corresponding buffers. The experiment was repeated with SEC purified CtxA WT with the same reaction set up except for a higher CtxA concentration (84 µM) but no difference in fluorescence signals was seen (data not shown).

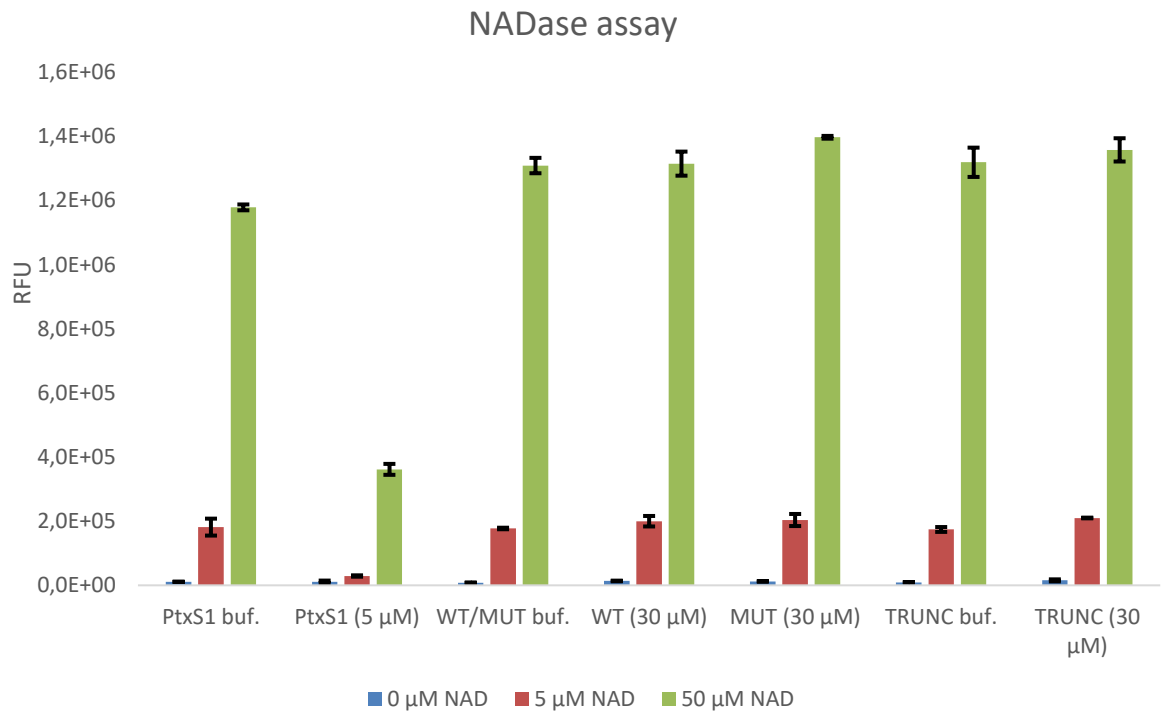

Figure 21. NADase consumption assay of 30 µM Ni-NTA purified CtxA 1-1C WT, MUT, and TRUNC. *Buf. means buffer. CtxA WT and MUT had the same buffer whereas CtxA TRUNC had a distinctive buffer. 0, 5 and 50 µM of ß-NAD^+ was used as a substrate for the hydrolysis reaction. The fluorescent signal of the fluorophore is measured as RFU with the Hidex Sense microplate reader. Excitation was set at 355 nm and emission at 485 nm. Error bars are set as standard deviation from the measured triplicate signals.*

4.7 CtxA is a novel bARTT, the target substrate is not found.

The first ADP-ribosylation studies were done with pooled Ni-NTA eluates of CtxA 1-1C WT, MUT and TRUNC utilizing biotin conjugated NAD^+ as the substrate. As it is generally known, the biotin-streptavidin interaction is one of the strongest non-covalent interactions which translates to the high sensitivity of the method (Chivers et al. 2011). The screening of putative bARTTs from bacterial lysates carried out at the beginning of the study indicated that CtxA 1-1C has auto ADP-ribosylation activity and that it is modified inside the bacterial cell during protein expression. To further study this phenomenon, biotin-NAD^+ was added to Ni-NTA purified proteins. As can be seen, CtxA 1-1C WT has a clear 25 kDa band on the streptavidin-HRP blot (Figure 22) and the intensity of the band is decreased substantially for CtxA 1-1C MUT. CtxA 1-1C TRUNC lost its activity despite also showing auto ADP-ribosylation activity in the bacterial lysate screening.

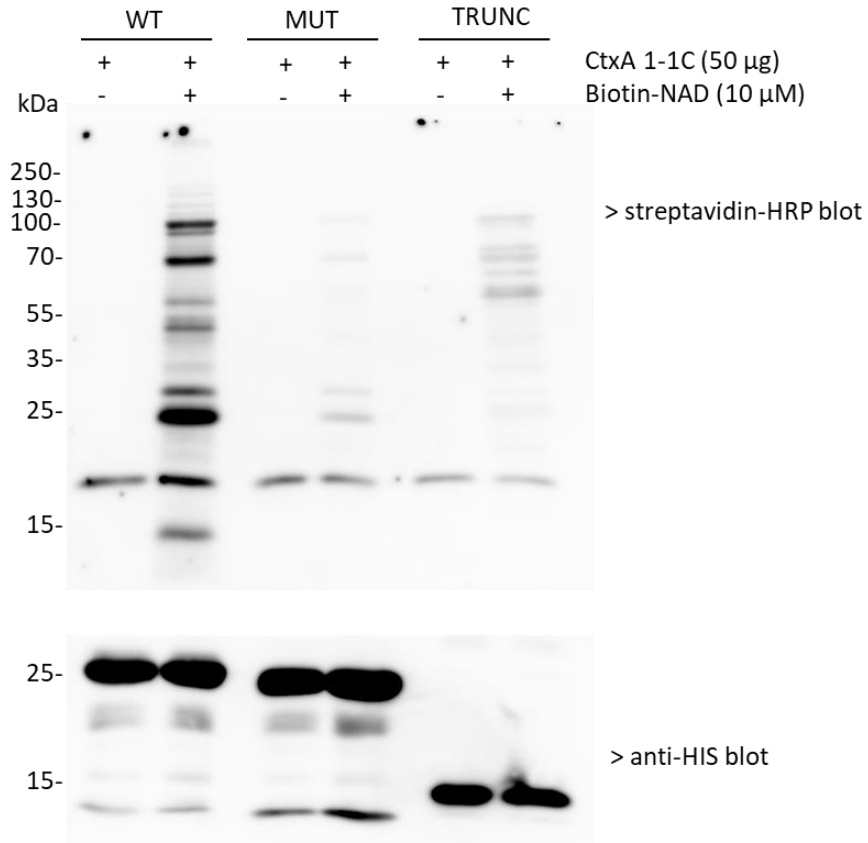

Figure 22. The auto ADP-ribosylation reaction of Ni-NTA purified CtxA 1-1C WT, MUT, and TRUNC. *10 µM of biotin-NAD^+ and 50 µg of protein was used in the reaction. For potential background signals, the proteins were incubated without biotin-NAD^+. An anti-His blot was used for verification of the streptavidin-HRP blot results. The 25 kDa*

band of CtxA 1-1C is clear meaning it has bound biotin-NAD^+. The mutated protein has decreased enzymatic activity towards biotin-NAD^+ whereas the 14 kDa CtxA TRUNC has no corresponding band on the streptavidin-HRP blot despite it being loaded according to the anti-His blot.

CtxA 1-1C WT was further purified with SEC and studied to see whether it maintained its auto ADP-ribosylation activity. This time, a common ADP-ribosylation inhibitor benzamide was used to see if the enzymatic reaction could be blocked. CtxA retained its enzymatic activity (Figure 23 A). Interestingly a 50 kDa band appeared on the streptavidin-HRP blot that is also seen on the anti-His blot. The automodification reaction was successfully inhibited by benzamide as the band intensity was reduced. Additionally, the faint 50 kDa band disappeared.

Inspired by this, further studies were conducted *in vitro* to identify potential target substrates in lysed eukaryotic cell lines of human embryonic kidney cells (HEK293T) and murine macrophage cells (RAW264.7). As expected, both soluble lysates of HEK293T and RAW264.7 showed no signal when incubated alone (Figure 23 B-C). After adding the enzyme CtxA 1-1C WT, more bands started appearing in both blots. The potential 50 kDa dimer band of CtxA had higher intensity. Bands between 70 – 100 kDa in size also appeared. This could be an indication of novel targets for CtxA 1-1C. The addition of the common inhibitor benzamide made the signals more faint which could indicate an enzymatically catalysed ADP-ribosylation reaction between CtxA and cell lysate proteins of HEK293T and RAW264.7.

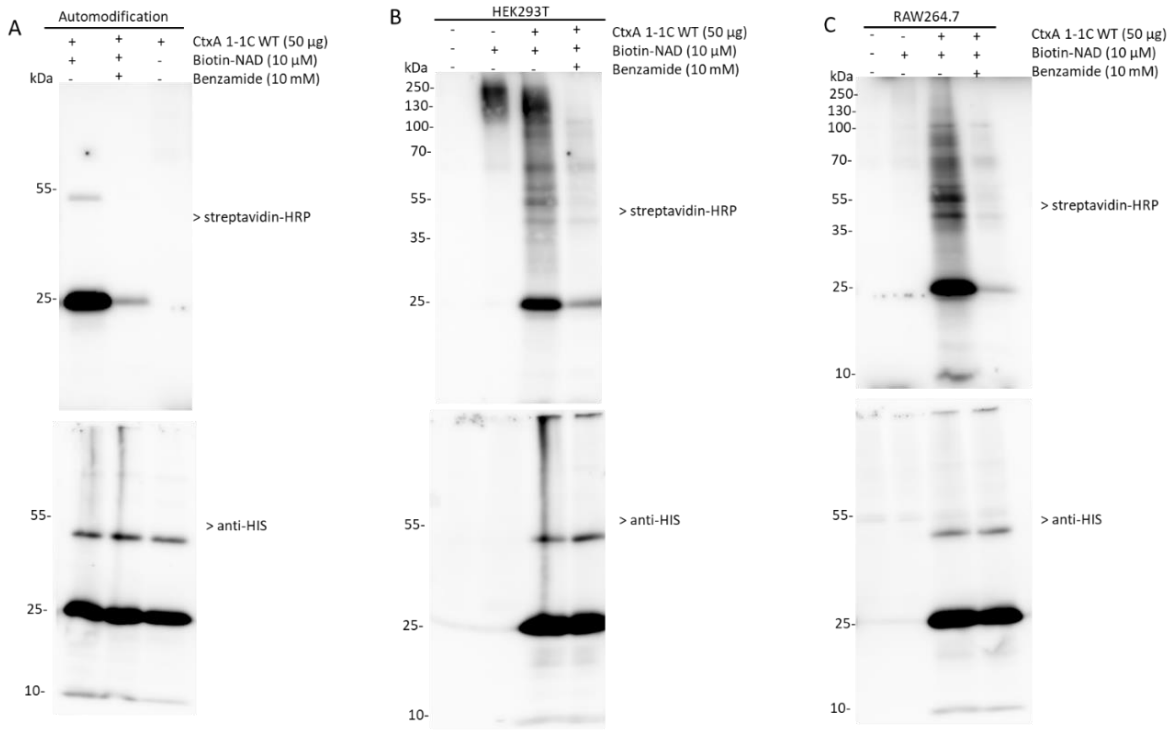

Figure 23. Activity and substrate studies of SEC purified CtxA 1-1C WT. (A) *The automodification (auto ADP-ribosylation) activity of CtxA 1-1C WT was studied with biotin-NAD⁺. Benzamide was used as an ADP-ribosylation reaction inhibitor. + and - signs indicate which reagents were added into the in vitro reaction. A 50 kDa dimer is seen on the streptavidin-HRP blot. It is also seen on the anti-His blot.* ***(B)*** *Human embryonic kidney (HEK293T) soluble cell lysates were added in the in vitro reaction to study potential target substrates. A high molecular weight band can be seen when HEK293T is incubated with biotin-NAD⁺. When CtxA 1-1C is added, more bands appear between 70 – 100 kDa and the reaction can be inhibited with benzamide.* ***(C)*** *The same result can be seen when the experiment is done under the same conditions but the with murine macrophage (RAW 264.7) cell line. In RAW264.7 there is no high molecular weight band seen when the cells are incubated with biotin-NAD⁺.*

To gain further affirmation that CtxA 1-1C has novel substrates in HEK293T and RAW264.7 cells, the *in vitro* reaction was repeated with conventional β-NAD⁺. There is always a possibility that biotin-NAD⁺, despite having high sensitivity, may give me mere artefacts as results. As can be seen from the anti-MAR/PAR blot (Figure 24) there are no clearly distinguishable, or novel bands seen either in the case of HEK293T or RAW264.7. There may be some novel substrate recognition at 70 – 100 kDa as seen in the streptavidin-HRP blot (Figure 23). On the contrary, in comparison to the

streptavidin-HRP blot, the automodification of CtxA in the anti-MAR/PAR blot is overwhelmingly strong and none of the reactions could be inhibited with benzamide (Figure 24).

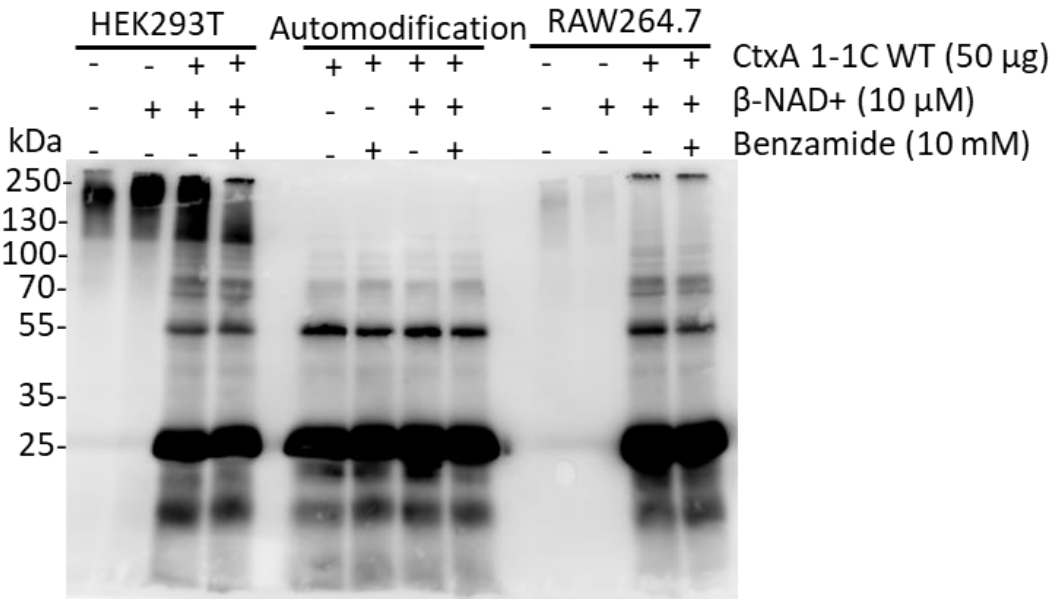

Figure 24. Substrate studies of SEC purified CtxA 1-1C WT conducted in HEK293T and RAW264.7 cell lysates. *Conventional β-NAD⁺ was used instead of biotin-NAD⁺. The membrane was blotted with an anti-MAR/PAR antibody. The high molecular weight band of HEK293T cells is visible but in the case of RAW264.7 cells it is not. When enzyme is added no clear bands can be seen but rather a smear. The automodification of CtxA is strong, and attempting to inhibit it with benzamide rendered no loss in activity. Bands between 70 – 100 kDa in size can be seen in the automodification reaction.*

5 Discussion

5.1 *Bartonella* ART screening analysis

ADP-ribosylation is a chemical modification of covalently adding an ADP-ribose moiety to the target substrate in the presence of NAD^+. It is a way of function for a large bacterial exotoxin group consisting of bacterial ADP-ribosyltransferase toxins called bARTTs. In this thesis, I provide compelling evidence that the *Bartonella sp. 1-1C* derived protein is a novel ADP-ribosylating exotoxin.

Four *Bartonella* species were screened for the putative exotoxin open reading frames found in their genomes. A small-scale (5 mL) expression system was set-up for skimming through bacterial lysates for toxins with ADP-ribosylation. As many ARTs possess auto-ADP-ribosylation activity, this experimentation method is fast and saves time and labour in comparison to individually expressing the proteins of interest and purifying them for further functionality studies.

On the anti-MAR/PAR blot, the wildtype proteins gave high-intensity bands corresponding to their predicted molecular weight except for the CtxA of *B. senegalensis* and *B. bovis* (Figure 10 A). The CtxA of *B. senegalensis* either has lower auto-ADP-ribosylation activity compared to other proteins or it does not have it at all. On the other hand, the CtxA of *B. senegalensis* may ADP-ribosylate a target protein in the bacterial lysate, hence the occurrence of the high intensity band at 55 kDa. The CtxA of *B. bovis* was expressed with an MBP-solubility tag, thus increasing its molecular weight. The correct 50 kDa band was not seen, indicating that the protein was inactive. However, a smaller 25 kDa band was seen which was distinctive from the empty control plasmid. It is possible that the solubility tag was cleaved off and that in reality the CtxA of *B. bovis* has automodification activity. Ideally the CtxA of *B. bovis* should be His-tagged to better understand its function or mutated to be able to compare its enzymatic activity side by side with the wildtype protein.

CtxA 1-1C remained soluble and active after the bacterial lysates were cleared by centrifugation (Figure 10 B). This made CtxA 1-1C a natural choice for further experiments as there was no need to drastically change the buffer compositions of the used lysis buffer. Additionally, this experiment indicated that CtxA 1-1C is a novel

bARTT because the mutations in CtxA MUT were in catalytically important amino acids. Moreover, the experiment suggested that CtxA 1-1C has automodification activity, and it is modified inside the bacterial expression host.

5.2 AlphaFold predicted CtxA 1-1C to be a CT-like toxin

I was interested in the fold of the CtxA 1-1C. Since crystallizing it would not be possible during my thesis, the fold was predicted using AlphaFold 2.0, an artificial intelligence-based software, that predicts the fold of a protein merely based on its primary amino acid sequence. AlphaFold predicted CtxA 1-1C to be a globular protein (Figure 11 A). It has perpendicular β-sheets and a variable number of α-helices which is a characteristic of a bARTT (Han and Tainer 2001). The blue α-helix (Figure 11 B) represents the A1 subunit of CT and LT proteins (Heggelund et al. 2015) which indicates that CtxA 1-1C could be a dual-chain protein. If this is the case, CtxA 1-1C should have a receptor binding B subunit CtxB making it an AB_5-toxin belonging to CT-like toxins. CtxA 1-1C was predicted to have an RSE catalytic motif (Figure 11 C-D) through a multiple sequence alignment study that is not presented in this thesis. Nevertheless, the superimposing of the catalytic CTA1 structure bound to NAD^+ with CtxA showed no structural mismatches, indicating that the catalytic cleft of CT and CtxA 1-1C are similar. These findings gave me confidence that CtxA 1-1C has an RSE motif, and within it an EXE motif containing the invariant glutamate common in all ARTs.

5.3 Purification of CtxA 1-1C

Inspired by the results above, I expressed CtxA 1-1C WT, MUT and TRUNC in large-scale using AIM and purified the proteins with Ni-NTA immobilized metal affinity chromatography as they are N-terminally His-tagged. There is always a potential risk involved in expressing toxins endogenously in a foreign host but fortunately *E. coli* BL21-DE3 proved to be a suitable host as the proteins were not toxic for the cells. This, however, does not explain the two-fold lower yields of CtxA MUT and TRUNC in comparison to WT despite all aforementioned proteins having the same culturing conditions. One explanation could be that mutating or truncating the protein affects its folding during expression. This could also explain the level of impurity of CtxA TRUNC in the PAGEBlue stain to a point where no correct molecular weight for the product

could be seen with the naked eye (Figure 14). The CtxA TRUNC yield loss could also be seen during purification steps as during flow-through a notable amount of protein was not captured by the beads. Since the protein expression strain BL21-DE3 could tolerate the different forms of CtxA, total protein yield could possibly be increased through a conventional culturing method using IPTG-induction.

CtxA WT, MUT, and TRUNC were further purified with size-exclusion chromatography (SEC) to remove the impurities of Ni-NTA purification. Previously, CtxA WT was purified with an S-200 column having a fractionation range of 5 – 250 kDa. This however made the protein elute in the void volume V_0. I was successful in overcoming this issue by using an S-400 column with a larger fractionation range.

One intriguing question is why CtxA eluted in the void volume V_0 in the first place. There could be numerous reasons for this such as the buffer conditions where the pH was altered or improper. Thus, it is possible that the used buffer rendered the protein unstable. Additionally, the buffer components and the use of detergents such NP-40 may have affected how the proteins move in the mobile phase. If this proves to be the case, diluting or replacing the detergent could improve the quality of the chromatogram. Another possibility is that the protein has higher oligomerisation states or that it has unspecific interactions with the column matrix.

When performing SEC, the general assumption is that all the molecules have the same symmetrical shape in the solution, meaning in my case that the protein is globular. However, some asymmetry may be present in the solution especially if the protein is not properly folded, has been modified i.e., glucosylated or if it is intrinsically disordered (Walls and Walker 2017). This results in the proteins eluting at an anomalously high molecular weight compared to a symmetrical globular protein with the same molecular weight. Nevertheless, buffer conditions could be checked for further optimization and if there is no room for improvement, changing the purification method could help shed light on the native state of the protein. Multiangle light scattering is also an option to study the native fold of the protein. Lastly, the failure to purify CtxA TRUNC could be explained by two factors: the usage of an improper column as the protein is 14 kDa in size and the fact that truncation could have simply made the protein unstable enough for it to be further fragmented during the purification process.

5.4 Characterisation of CtxA 1-1C

After purification, the first characterization step was performing differential scanning fluorimetry (DSF) or a thermal shift assay to study the folding of the SEC purified proteins in their corresponding buffers. DSF utilizes a fluorescent dye SYPRO Orange that binds to the hydrophobic amino acid residues during protein unfolding. As can be seen in figure 19, CtxA WT and MUT had peculiar curves, which would support the idea that these proteins are not properly folded, hence the uncharacteristic behaviour during SEC purification. Then again, the improper curves and high T_m values may have a more rational explanation. SYPRO Orange is susceptible to detergents and the increased background signal may be due to the NP-40 contained in the buffers of CtxA WT and MUT. Nonetheless, this indicates that a proper buffer screening would have been necessary. The detergent background seen with SYPRO Orange could also be avoided by switching the fluorescent dye to one that detergents do not interfere with such as 8-Anilinonaphthalene-1-sulfonic acid (1-ANS) (Semisotnov et al. 1991). As for arguing whether the used method or instrument worked at all, the T_m value of the used control PtxS1 was 53,5 °C compared to the T_m value 54,7 ± 0,2 °C in the paper by Ashok et al. (2020).

The NADase consumption assay was performed to gain insight into whether CtxA 1-1C has natural NAD^+ hydrolase activity such as PtxS1 does for example. This was done as an endpoint fluorometric assay where the unconsumed NAD^+ was converted in a two-step reaction to a detectable fluorophore. Underwhelmingly, CtxA did not show NADase activity (Figure 21) but instead exhibited even higher fluorescence values than the buffer controls. It could be possible that the assay lacks the sensitivity needed to detect the alterations in NAD^+ consumption. Inhibiting the automodification reaction during expression with a competitive inhibitor and repeating the NADase setup would give a clearer picture of how CtxA hydrolyses NAD^+. It is more likely that CtxA 1-1C needs its target substrate to show any indications of NADase activity.

The screening of bacterial lysates in the beginning of the study provided me with hints that CtxA 1-1C has robust automodification activity. The following NADase assay gave me further indications of this activity since the RFU values were even higher when enzyme was added compared to buffer only controls. To gain further proof of the

automodification activity, CtxA WT, MUT and TRUNC were purified, and their enzymatic activity studied with biotin-NAD^+. Additionally, CtxA WT was studied with conventional β-NAD^+. As figure 22 indicates, the automodification activity is reduced explicitly when the protein was mutated, which is in line with how enzymes belonging to ARTs behave. Mutating the residues of the catalytic EXE-motif result in up to 1000-fold decrease in ADP-ribosylation activity (Simon et al. 2014). In my studies CtxA TRUNC lost its automodification activity despite showing hints that it might possess this activity in the bacterial lysate study (Figure 10). This provides further evidence that either the truncation of CtxA TRUNC extends too far for its binding pocket to hold biotin-NAD^+ in place or the truncation rendered the enzyme inactive.

Lastly, the SEC-purified CtxA WT was used for eukaryotic cell lysate studies as it is free from possibly inhibiting impurities that would mask the background. An in vitro set up was created to study whether the enzyme modifies any substrates from lysed eukaryotic HEK293T and RAW264.7 cells. The experiment was initially conducted with biotin-NAD^+ because of the high sensitivity of the western blot assay when streptavidin-HRP is added. Hence, the potential target substrates should be visible on the western blot even in low enzyme and lysate quantities. After finding potential target substrates, the experiment is repeated with conventional β-NAD^+. This ensures that I do not see mere artefacts on the biotin-NAD^+ blot such streptavidin-derived unspecific interactions.

The results from the biotin-NAD^+ experiment proved to be compelling as there were novel bands on the western blot that did not appear when the eukaryotic lysates were incubated alone or with biotin-NAD^+ (Figure 23 B-C). Furthermore, the competitive inhibitor benzamide was able to reduce signal intensities. When switching to the conventional β-NAD^+, the results were underwhelming in light of finding a potential substrate from either HEK293T or RAW264.7 cells. No clear bands showed up and the automodification of CtxA exhibited potentially higher multimerization states (Figure 24). This could indicate that CtxA 1-1C and the potential eukaryotic target substrates have completely different affinity to β-NAD^+. This could also explain why the automodication activity could not be inhibited with benzamide: the affinity of β-NAD^+ is so strong that benzamide is not able to compete with it in the active site.

All in all, my studies strongly indicate that CtxA 1-1C is a 25 kDa protein belonging to bARTTs. It has an RSE catalytic motif which classifies it as a CT-like toxin. The DSF results left a lot to be desired as the detergent in the buffer interfered with the fluorescent dye. Furthermore, in contrast to PtxS1, CtxA 1-1C does not seem to have NADase activity nor was I able to find its target substrate in the used eukaryotic cell lines or within the scope of the *in vitro* experiment setup. I would have needed a method for identifying the bands, had I found potential protein target substrates from the eukaryotic cell lines used for the western blots. This could have been done with mass spectrometry although the complex nature of ADP-ribosylation demands more sophisticated analysis methods (Rosenthal et al. 2015).

6 Conclusion and future studies

Overall, this thesis study provides compelling evidence that CtxA of *Bartonella sp. 1-1C* is a novel bARTT with auto ADP-ribosylation activity. An important question regarding future studies is which amino acid residues CtxA modifies on itself. To explore this question automodification reactions with β-NAD^+ could be carried out and the samples could be analysed with mass spectrometry. This could also aid in finding potential target substrate proteins that undergo modification by CtxA.

One perhaps more important obstacle to overcome in the future is the optimization of buffer conditions for CtxA 1-1C and defining its native structure. Additionally, further studies could explore the effects of inhibiting the automodification activity of CtxA by adding a competitive inhibitor such as benzamide during the protein expression step. The overall experiment set up could also be improved and more information could be gained if the experiments were done *in vivo*. This would require the presence of the receptor binding B subunit CtxB and some way of localizing CtxA once it is inside the cell. Could interactions between CtxB with CtxA provide more insights about CtxA? This is a question worth exploring postulating of course that the bARTT of *Bartonella sp. 1-1C* is a CT-like toxin having an AB_5-like structure, something that the AlphaFold model leans towards.

References

Allured, V. S., Collier, R. J., Carroll, S. F. & McKay, D. B. (1986) Structure of exotoxin A of Pseudomonas aeruginosa at 3.0-Angstrom resolution. *Proc Natl Acad Sci U S A* **83**:1320–1324.

Armstrong, G. D., Howard, L. A. & Peppler, M. S. (1988) Use of glycosyltransferases to restore pertussis toxin receptor activity to asialoagalactofetuin. *J Biol Chem* **263**:8677–8684.

Ashok, Y., Miettinen, M., Oliveira, D. K. H. De, Tamirat, M. Z., Näreoja, K., Tiwari, A., Hottiger, M. O., Johnson, M. S., Lehtiö, L. & Pulliainen, A. T. (2020) Discovery of compounds inhibiting the ADP-ribosyltransferase activity of pertussis toxin. *ACS Infect Dis* **6**:588–602.

Barton, A. L. (1909) Descripcion de elementos endoglobulares hallados en los enfermos de fiebre verrucoca. *La Crónica Médica Lima* **26**:7–10.

Bell, C. E. & Eisenberg, D. (1997) Crystal structure of diphtheria toxin bound to nicotinamide adenine dinucleotide. *Adv Exp Med Biol* **419**:35–43.

Brouqui, P., Lascola, B., Roux, V. & Raoult, D. (1999) Chronic Bartonella quintana bacteremia in homeless patients. *N Engl J Med* **340**:184–189.

Burnette, W. N., Cieplak, W., Mar, V. L., Kaljot, K. T., Sato, H. & Keith, J. M. (1988) Pertussis toxin S1 mutant with reduced enzyme activity and a conserved protective epitope. *Science (80-)* **242**:72–74.

Burnette, W. N., Mar, V. L., Platler, B. W., Schlotterbeck, J. D., McGinley, M. D., Stoney, K. S., Rohde, M. F. & Kaslow, H. R. (1991) Site-specific mutagenesis of the catalytic subunit of cholera toxin: Substituting lysine for arginine 7 causes loss of activity. *Infect Immun* **59**:4266–4270.

Byam, W. & Lloyd, L. L. (1920) Trench fever: Its epidemiology and endemiology. *Proc R Soc Med* **13**:1–27.

Carroll, S. F. & Collier, R. J. (1984) NAD binding site of diphtheria toxin: Identification of a residue within the nicotinamide subsite by photochemical modification with NAD. *Proc Natl Acad Sci U S A* **81**:3307–3311.

Carroll, S. F. & Collier, R. J. (1987) Active site of Pseudomonas aeruginosa exotoxin A. Glutamic acid 553 is photolabeled by NAD and shows functional homology with glutamic acid 148 of diphtheria toxin. *J Biol Chem* **262**:8707–8711.

Carroll, S. F. & Collier, R. J. (1988) Amino acid sequence homology between the enzymic domains of diphtheria toxin and Pseudomonas aeruginosa exotoxin A. *Mol Microbiol* **2**:293–296.

Cassel, D. & Pfeuffer, T. (1978) Mechanism of cholera toxin action: Covalent modification of the guanyl nucleotide-binding protein of the adenylate cyclase system. *Proc Natl Acad Sci U S A* **75**:2669–2673.

Chambon, P., Weill, J. . & Mandel, P. (1963) Nicotinamide mononucleotide activation of a new DNA-dependent polyadenylic acid synthesizing nuclear enzyme. *Biochem*

Biophys Res Commun **11**:39–43.

Chaudhary, V. K., Jinno, Y., Fitzgerald, D. & Pastan, I. R. A. (1990) Pseudomonas exotoxin contains a specific sequence at the carboxyl terminus that is required for cytotoxicity. *Proc Natl Acad Sci U S A* **87**:308–312.

Chenal, A., Savarin, P., Nizard, P., Guillain, F., Gillet, D. & Forge, V. (2002) Membrane protein insertion regulated by bringing electrostatic and hydrophobic interactions into play. *J Biol Chem* **277**:43425–43432.

Chinnapen, D. J. F., Hsieh, W. T., te Welscher, Y. M., Saslowsky, D. E., Kaoutzani, L., Brandsma, E., D'Auria, L., Park, H., Wagner, J. S., Drake, K. R., Kang, M., Benjamin, T., Ullman, M. D., Costello, C. E., Kenworthy, A. K., Baumgart, T., Massol, R. H. & Lencer, W. I. (2012) Lipid Sorting by Ceramide Structure from Plasma Membrane to ER for the Cholera Toxin Receptor Ganglioside GM1. *Dev Cell* **23**:573–586.

Chiron, M. F., Fryling, C. M. & Fitzgerald, D. J. (1994) Cleavage of pseudomonas exotoxin and diphtheria toxin by a furin-like enzyme prepared from beef liver. *J Biol Chem* **269**:18167–18176.

Chivers, C. E., Koner, A. L., Lowe, E. D. & Howarth, M. (2011) How the biotin-streptavidin interaction was made even stronger: Investigation via crystallography and a chimaeric tetramer. *Biochem J* **435**:55–63.

Cho, C. C., Chien, C. Y., Chiu, Y. C., Lin, M. H. & Hsu, C. H. (2019) Structural and biochemical evidence supporting poly ADP-ribosylation in the bacterium Deinococcus radiodurans. *Nat Commun* **10**:1–14.

Choe, S., Bennett, M. J., Fujii, G., Curmi, P. M. G., Kantardjieff, K. A., Collier, R. J. & Eisenberg, D. (1992) The crystal structure of diphtheria toxin. *Nature* **357**:216–222.

Chomel, B. B., Kasten, R. W., Floyd-Hawkins, K., Chi, B., Yamamoto, K., Roberts-Wilson, J., Gurfield, A. N., Abbott, R. C., Pedersen, N. C. & Koehler, J. E. (1996) Experimental transmission of Bartonella henselae by the cat flea. *J Clin Microbiol* **34**:1952–1956.

Culver, G. M., McCraith, S. M., Zillmann, M., Kierzek, R., Michaud, N., LaReau, R. D., Turner, D. H. & Phizicky, E. M. (1993) An NAD derivative produced during transfer RNA splicing: ADP-ribose 1"-2" cyclic phosphate. *Science (80-)* **261**:206–208.

Dabbs, E. R., Yazawa, K., Mikami, Y., Miyaji, M., Morisaki, N., Iwasaki, S. & Furihata, K. (1995) Ribosylation by mycobacterial strains as a new mechanism of rifampin inactivation. *Antimicrob Agents Chemother* **39**:1007–1009.

Dolan, K. M., Lindenmayer, G. & Olson, J. C. (2000) Functional comparison of the NAD binding cleft of ADP-ribosylating toxins. *Biochemistry* **39**:8266–8275.

Domenighini, M., Magagnoli, C., Pizza, M. & Rappuoli, R. (1994) Common features of the NAD-binding and catalytic site of ADP-ribosylating toxins. *Mol Microbiol* **14**:41–50.

Domenighini, M. & Rappuoli, R. (1996) Three conserved consensus sequences identify the NAD-binding site of ADP-ribosylating enzymes, expressed by eukaryotes, bacteria and T-even bacteriophages. *Mol Microbiol* 667–674.

Engel, P., Salzburger, W., Liesch, M., Chang, C. C., Maruyama, S., Lanz, C., Calteau, A., Lajus, A., Médigue, C., Schuster, S. C. & Dehio, C. (2011) Parallel evolution of a type IV

secretion system in radiating lineages of the host-restricted bacterial pathogen bartonella. *PLoS Genet* **7**:.

Eremeeva, M. E., Gerns, H. L., Lydy, S. L., Goo, J. S., Ryan, E. T., Mathew, S. S., Ferraro, M. J., Holden, J. M., Nicholson, W. L., Dasch, G. A. & Koehler, J. E. (2007) Bacteremia, Fever, and Splenomegaly Caused by a Newly Recognized Bartonella Species. *N Engl J Med* **356**:2381–2387.

Falnes, P., Ariansen, S., Sandvig, K. & Olsnes, S. (2000) Requirement for prolonged action in the cytosol for optimal protein synthesis inhibition by diphtheria toxin. *J Biol Chem* **275**:4363–4368.

Falnes, P. O. & Olsnes, S. (1995) Cell-mediated reduction and incomplete membrane translocation of diphtheria toxin mutants with internal disulfides in the A fragment. *J Biol Chem* **270**:20787–20793.

Fieldhouse, R. J., Jørgensen, R., Lugo, M. R. & Merrill, A. R. (2012) The 1.8 A Cholix toxin crystal structure in complex with NAD+ and evidence for a new kinetic mode. *J Biol Chem* **287**:21176–21188.

Flexman, J. P., Lavis, N. J., Kay, I. D., Watson, M., Metcalf, C. & Pearman, J. W. (1995) Bartonella henselae is a causative agent of cat scratch disease in Australia. *J Infect* **31**:241–245.

Foil, L., Andress, E., Freeland, R. L., Roy, A. F., Rutledge, R., Triche, P. C. & O'Reilly, K. L. (1998) Experimental Infection of Domestic Cats with Bartonella henselae by Inoculation of Ctenocephalides felis (Siphonaptera: Pulicidae) Feces. *J Med Entomol* **35**:625–628.

Garcia-Quintanilla, M., Dichter, A. A., Guerra, H. & Kempf, V. A. J. (2019) Carrion's disease: More than a neglected disease. *Parasites and Vectors* . BioMed Central 1–12.

García-Saura, A. G., Zapata-Pérez, R., Hidalgo, J. F. & Sánchez-Ferrer, Á. (2018) Comparative inhibitory profile and distribution of bacterial PARPs, using Clostridioides difficile CD160 PARP as a model. *Sci Rep* **8**:1–12.

Gasquet, S., Maurin, M., Brouqui, P., Lepidi, H. & Raoult, D. (1998) Bacillary angiomatosis in immunocompromised patients. *Aids* **12**:1793–1803.

Gibrat, J. F., Madej, T. & Bryant, S. H. (1996) Surprising similarities in structure comparison. *Curr Opin Struct Biol* **6**:377–385.

Gill, D. M. & Meren, R. (1978) ADP-ribosylation of membrane proteins catalyzed by cholera toxin: basis of the activation of adenylate cyclase. *Proc Natl Acad Sci U S A* **75**:3050–3054.

Gillet, D. & Barbier, J. (2015) 4 - Diphtheria toxin. in Alouf, J., Ladant, D. and Popoff, M. R. B. T.-T. C. S. of B. P. T. (Fourth E. (eds). Academic Press, Boston 111–132.

Goor, R. S., Pappenheimer, A. M. & Ames, E. (1967) Studies on the mode of action of diphtheria toxin V. Inhibition of peptide bond formation by toxins and NAD in cell-free systems and its reversal by nicotinamide 923–939.

Gülke, I., Pfeifer, G., Liese, J., Fritz, M., Hofmann, F., Aktories, K. & Barth, H. (2001) Characterization of the enzymatic component of the ADP-ribosyltransferase toxin CDTa

from Clostridium difficile. *Infect Immun* **69**:6004–6011.

Han, S. & Tainer, J. A. (2001) The ARTT motif and a unified structural understanding of substrate recognition in ADP-ribosylating bacterial toxins and eukaryotic ADP-ribosyltransferases. *Int J Med Microbiol* **291**:523–529.

Han, X. Y. & Galloway, D. R. (1995) Active site mutations of Pseudomonas aeruginosa exotoxin A. Analysis of the His440 residue. *J Biol Chem* **270**:679–684.

Harms, A., Segers, F. H. I. D., Quebatte, M., Mistl, C., Manfredi, P., Körner, J., Chomel, B. B., Kosoy, M., Maruyama, S., Engel, P. & Dehio, C. (2017) Evolutionary dynamics of pathoadaptation revealed by three independent acquisitions of the VirB/D4 type IV secretion system in Bartonella. *Genome Biol Evol* **9**:761–776.

Harper, C. B., McCluskey, A., Robinson, P. J. & Meunier, F. A. (2015) 37 - Exploiting endocytic pathways to prevent bacterial toxin infection. in Alouf, J., Ladant, D. and Popoff, M. R. B. T.-T. C. S. of B. P. T. (Fourth E. (eds) *Compr Sourceb Bact Protein Toxins (Fourth Ed* . Academic Press, Boston 1072–1094.

Hausman, S. Z. & Burns, D. L. (1993) Binding of pertussis toxin to lipid vesicles containing glycolipids. *Infect Immun* **61**:335–337.

Hazes, B. & Read, R. J. (1997) Accumulating evidence suggests that several AB-toxins subvert the endoplasmic reticulum-associated protein degradation pathway to enter target cells. *Biochemistry* **36**:11051–11054.

Heggelund, J. E., Bjørnestad, V. A. & Krengel, U. (2015) 7 - Vibrio cholerae and Escherichia coli heat-labile enterotoxins and beyond. in Alouf, J., Ladant, D. and Popoff, M. R. B. T.-T. C. S. of B. P. T. (Fourth E. (eds). Academic Press, Boston 195–229.

Holmgren, J., Fredman, P., Lindblad, M., Svennerholm, A. M. & Svennerholm, L. (1982) Rabbit intestinal glycoprotein receptor for Escherichia coli heat-labile enterotoxin lacking affinity for cholera toxin. *Infect Immun* **38**:424–433.

Holmgren, J., Lonnroth, I., Mansson, J. E. & Svennerholm, L. (1975) Interaction of cholera toxin and membrane GM1 ganglioside of small intestine. *Proc Natl Acad Sci U S A* **72**:2520–2524.

Honjo, T., Nishizuka, Y. & Hayaishi, O. (1968) Diphtheria toxin-dependent adenosine diphosphate ribosylation of aminoacyl transferase II and inhibition of protein synthesis. *J Biol Chem* **243**:3553–3555.

Iglesias-Bartolomé, R., Trenchi, A., Comín, R., Moyano, A. L., Nores, G. A. & Daniotti, J. L. (2009) Differential endocytic trafficking of neuropathy-associated antibodies to GM1 ganglioside and cholera toxin in epithelial and neural cells. *Biochim Biophys Acta - Biomembr* **1788**:2526–2540.

Inocencio, N. M., Moehring, J. M. & Moehring, T. J. (1994) Furin activates Pseudomonas exotoxin A by specific cleavage in vivo and in vitro. *J Biol Chem* **269**:31831–31835.

Inoue, K., Maruyama, S., Kabeya, H., Hagiya, K., Izumi, Y., Une, Y. & Yoshikawa, Y. (2009) Exotic small mammals as potential reservoirs of zoonotic Bartonella spp. *Emerg Infect Dis* **15**:526–532.

Jacomo, V., Kelly, P. J. & Raoult, D. (2002) Natural history of Bartonella infections (an exception to Koch's postulate). *Clin Diagn Lab Immunol* **9**:8–18.

Jankevicius, G., Ariza, A., Ahel, M. & Ahel, I. (2016) The toxin-antitoxin system DarTG catalyzes reversible ADP-ribosylation of DNA. *Mol Cell* **64**:1109–1116.

Jørgensen, R., Merrill, A. R., Yates, S. P., Marquez, V. E., Schwan, A. L., Boesen, T. & Andersen, G. R. (2005) Exotoxin A-eEF2 complex structure indicates ADP ribosylation by ribosome mimicry. *Nature* **436**:979–984.

Jørgensen, R., Purdy, A. E., Fieldhouse, R. J., Kimber, M. S., Bartlett, D. H. & Merrill, A. R. (2008) Cholix toxin, a novel ADP-ribosylating factor from Vibrio cholerae. *J Biol Chem* **283**:10671–10678.

Jumper, J., Evans, R., Pritzel, A., Green, T., Figurnov, M., Ronneberger, O., Tunyasuvunakool, K., Bates, R., Žídek, A., Potapenko, A., Bridgland, A., Meyer, C., Kohl, S. A. A., Ballard, A. J., Cowie, A., Romera-Paredes, B., Nikolov, S., Jain, R., Adler, J. et al. (2021) Highly accurate protein structure prediction with AlphaFold. *Nature* **596**:583–589.

Katada, T. & Ui, M. (1981) Islet-activating protein. A modifier of receptor-mediated regulation of rat islet adenylate cyclase. *J Biol Chem* **256**:8310–8317.

Koehler, J. E., Glaser, C. A. & Tappero, J. W. (1994) Rochalimaea henselae Infection: A New Zoonosis With the Domestic Cat as Reservoir. *JAMA* **271**:531–535.

Kounnas, M. Z., Morris, R. E., Thompson, M. R., FitzGerald, D. J., Strickland, D. K. & Saelinger, C. B. (1992) The α2-macroglobulin receptor/low density lipoprotein receptor-related protein binds and internalizes Pseudomonas exotoxin A. *J Biol Chem* **267**:12420–12423.

Krügel, M., Król, N., Kempf, V. A. J., Pfeffer, M. & Obiegala, A. (2022) Emerging rodent-associated Bartonella: a threat for human health? *Parasites and Vectors* **15**:1–19.

Kufel, W. D., Devanathan, A. S., Marx, A. H., Weber, D. J. & Daniels, L. M. (2017) Bezlotoxumab: A Novel Agent for the Prevention of Recurrent Clostridium difficile Infection. *Pharmacotherapy* **37**:1298–1308.

Lemichez, E., Bomsel, M., Devilliers, G., Vanderspek, J., Murphy, J. R., Lukianov, E. V, Olsnes, S. & Boquet, P. (1997) Membrane translocation of diphtheria toxin fragment A exploits early to late endosome trafficking machinery. *Mol Biol* **23**:445–457.

Lencer, W. I., Constable, C., Moe, S., Jobling, M. G., Webb, H. M., Ruston, S., Madara, J. L., Hirst, T. R. & Holmes, R. K. (1995) Targeting of cholera toxin and Escherichia coli heat labile toxin in polarized epithelia: Role of COOH-terminal KDEL. *J Cell Biol* **131**:951–962.

Lesnick, M. L., Reiner, N. E., Fierer, J. & Guiney, D. G. (2001) The Salmonella spvB virulence gene encodes an enzyme that ADP-ribosylates actin and destabilizes the cytoskeleton of eukaryotic cells. *Mol Microbiol* **39**:1464–1470.

Li, M., Dyda, F., Benhar, I., Pastan, I. & Davies, D. R. (1996) Crystal structure of the catalytic domain of Pseudomonas exotoxin A complexed with a nicotinamide adenine dinucleotide analog: Implications for the activation process and for ADP ribosylation. *Proc Natl Acad Sci U S A* **93**:6902–6906.

Lin, J. W., Chen, C. Y., Chen, W. C., Chomel, B. B. & Chang, C. C. (2008) Isolation of Bartonella species from rodents in Taiwan including a strain closely related to 'Bartonella rochalimae' from Rattus norvegicus. *J Med Microbiol* **57**:1496–1501.

Lobet, Y., Cluff, C. W. & Cieplak, W. (1991) Effect of site-directed mutagenic alterations on ADP-ribosyltransferase activity of the A subunit of Escherichia coli heat-labile enterotoxin. *Infect Immun* **59**:2870–2879.

Locht, C. & Antoine, R. (1995) A proposed mechanism of ADP-ribosylation catalyzed by the pertussis toxin S1 subunit. *Biochimie* **77**:333–340.

Lüscher, B., Ahel, I., Altmeyer, M., Ashworth, A., Bai, P., Chang, P., Cohen, M., Corda, D., Dantzer, F., Daugherty, M. D., Dawson, T. M., Dawson, V. L., Deindl, S., Fehr, A. R., Feijs, K. L. H., Filippov, D. V., Gagné, J. P., Grimaldi, G., Guettler, S. et al. (2021) ADP-ribosyltransferases, an update on function and nomenclature. *FEBS J* 1–12.

Maggi, R. G., Duncan, A. W. & Breitschwerdt, E. B. (2005) Novel chemically modified liquid medium that will support the growth of seven Bartonella species. *J Clin Microbiol* **43**:2651–2655.

Majoul, I., Ferrari, D. & Söling, H. D. (1997) Reduction of protein disulfide bonds in an oxidizing environment. The disulfide bridge of cholera toxin A-subunit is reduced in the endoplasmic reticulum. *FEBS Lett* **401**:104–108.

Masignani, V., Balducci, E., Di Marcello, F., Savino, S., Serruto, D., Veggi, D., Bambini, S., Scarselli, M., Aricò, B., Comanducci, M., Adu-Bobie, J., Giuliani, M. M., Rappuoli, R. & Pizza, M. (2003) NarE: A novel ADP-ribosyltransferase from Neisseria meningitidis. *Mol Microbiol* **50**:1055–1067.

Masignani, V., Balducci, E., Serruto, D., Veggi, D., Aricò, B., Comanducci, M., Pizza, M. & Rappuoli, R. (2004) In silico identification of novel bacterial ADP-ribosyltransferases. *Int J Med Microbiol* **293**:471–478.

Masin, J., Osicka, R., Bumba, L., Sebo, P. & Locht, C. (2015) 6 - Bordetella protein toxins. in Alouf, J., Ladant, D. and Popoff, M. R. B. T.-T. C. S. of B. P. T. (Fourth E. (eds). Academic Press, Boston 161–194.

Maurin, M., Roux, V., Stein, A., Ferrier, F., Viraben, R. & Raoult, D. (1994) Isolation and characterization by immunofluorescence, sodium dodecyl sulfate-polyacrylamide gel electrophoresis, Western blot, restriction fragment length polymorphism-PCR, 16S rRNA gene sequencing, and pulsed-field gel electrophoresis of Rochalimaea quin. *J Clin Microbiol* **32**:1166–1171.

McKee, M. L. & FitzGerald, D. J. (1999) Reduction of furin-nicked Pseudomonas exotoxin A: An unfolding story. *Biochemistry* **38**:16507–16513.

Morrison, A. R., Moss, J., Stevens, L. A., Evans, J. E., Farrell, C., Merithew, E., Lambright, D. G., Greiner, D. L., Mordes, J. P., Rossini, A. A. & Bortell, R. (2006) ART2, a T cell surface mono-ADP-ribosyltransferase, generates extracellular poly(ADP-ribose). *J Biol Chem* **281**:33363–33372.

Moss, J. & Richardson, S. H. (1978) Activation of Adenylate Cyclase by Heat-Labile Escherichia Coli Enterotoxin. *J Clin Invest* **62**:281–285.

Moss, J. & Vaughan, M. (1977) Mechanism of action of choleragen. Evidence for ADP

ribosyltransferase activity with arginine as an acceptor. *J Biol Chem* **252**:2455–2457.

Mullins, K. E., Hang, J., Clifford, R. J., Onmus-Leone, F., Yang, Y., Jiang, J., Leguia, M., Kasper, M. R., Maguina, C., Lesho, E. P., Jarman, R. G., Richards, A. & Blazes, D. (2017) Whole-genome analysis of Bartonella ancashensis, a novel pathogen causing verruga Peruana, rural Ancash Region, Peru. *Emerg Infect Dis* **23**:430–438.

Naglich, J. G., Metherall, J. E., Russell, D. W. & Eidels, L. (1992) Expression cloning of a diphtheria toxin receptor: Identity with a heparin-binding EGF-like growth factor precursor. *Cell* **69**:1051–1061.

O'Neal, C. J., Jobling, M. G., Holmes, R. K. & Hol, W. G. J. (2005) Structural basis for the activation of cholera toxin by human ARF6-GTP. *Science (80-)* **309**:1093–1096.

Parte, A. C., Carbasse, J. S., Meier-Kolthoff, J. P., Reimer, L. C. & Göker, M. (2020) List of prokaryotic names with standing in nomenclature (LPSN) moves to the DSMZ. *Int J Syst Evol Microbiol* **70**:5607–5612.

Pavlovskis, O. R., Iglewski, B. H. & Pollack, M. (1978) Mechanism of action of Pseudomonas aeruginosa exotoxin A in experimental mouse infections: adenosine diphosphate ribosylation of elongation factor 2. *Infect Immun* **19**:29–33.

Pederson, K. J., Vallis, A. J., Aktories, K., Frank, D. W. & Barbieri, J. T. (1999) The amino-terminal domain of Pseudomonas aeruginosa ExoS disrupts actin filaments via small-molecular-weight GTP-binding proteins. *Mol Microbiol* **32**:393–401.

Perelle, S., Gibert, M., Bourlioux, P., Corthier, G. & Popoff, M. R. (1997) Production of a complete binary toxin (actin-specific ADP- ribosyltransferase) by Clostridium difficile CD196. *Infect Immun* **65**:1402–1407.

Perina, D., Mikoč, A., Ahel, J., Ćetković, H., Žaja, R. & Ahel, I. (2014) Distribution of protein poly(ADP-ribosyl)ation systems across all domains of life. *DNA Repair (Amst)* **23**:4–16.

Pescador Vargas, B. & Roa Culma, L. A. (2017) Pertussis: enfermedad reemergente. *Rev Med* **25**:78–95.

Picciotto, M. R., Cohn, J. A., Bertuzzi, G., Greengard, P. & Nairn, A. C. (1992) Phosphorylation of the cystic fibrosis transmembrane conductance regulator. *J Biol Chem* **267**:12742–12752.

Putt, K. S. & Hergenrother, P. J. (2004) An enzymatic assay for poly(ADP-ribose) polymerase-1 (PARP-1) via the chemical quantitation of NAD+: Application to the high-throughput screening of small molecules as potential inhibitors. *Anal Biochem* **326**:78–86.

Ratts, R., Zeng, H., Berg, E. A., Blue, C., McComb, M. E., Costello, C. E., VanderSpek, J. C. & Murphy, J. R. (2003) The cytosolic entry of diphtheria toxin catalytic domain requires a host cell cytosolic translocation factor complex. *J Cell Biol* **160**:1139–1150.

Ray, S., Taylor, M., Banerjee, T., Tatulian, S. A. & Teter, K. (2012) Lipid rafts alter the stability and activity of the cholera toxin A1 subunit. *J Biol Chem* **287**:30395–30405.

Rosenthal, F., Nanni, P., Barkow-Oesterreicher, S. & Hottiger, M. O. (2015) Optimization of LTQ-orbitrap mass spectrometer parameters for the identification of

ADP-ribosylation sites. *J Proteome Res* **14**:4072–4079.

Roussin, M. & Salcedo, S. P. (2021) NAD+-targeting by bacteria: An emerging weapon in pathogenesis. *FEMS Microbiol Rev* . Oxford University Press 1–20.

Sakari, M., Laisi, A. & Pulliainen, A. T. (2022) Exotoxin-Targeted Drug Modalities as Antibiotic Alternatives. *ACS Infect Dis* **8**:433–456.

Scherer, D. C., Deburon-Connors, I. & Minnick, M. F. (1993) Characterization of Bartonella bacilliformis flagella and effect of antiflagellin antibodies on invasion of human erythrocytes. *Infect Immun* **61**:4962–4971.

Scheuring, J. & Schramm, V. L. (1997) Pertussis toxin: Transition state analysis for ADP-ribosylation of G- protein peptide α(i3)C20. *Biochemistry* **36**:8215–8223.

Schülein, R., Seubert, A., Gille, C., Lanz, C., Hansmann, Y., Piémont, Y. & Dehio, C. (2001) Invasion and persistent intracellular colonization of erythrocytes: A unique parasitic strategy of the emerging pathogen Bartonella. *J Exp Med* **193**:1077–1086.

La Scola, B. & Raoult, D. (1999) Culture of Bartonella quintana and Bartonella henselae from human samples: A 5-year experience (1993 to 1998). *J Clin Microbiol* **37**:1899–1905.

Semisotnov, G. V., Rodionova, N. A., Razgulyaev, O. I., Uversky, V. N., Gripas', A. F. & Gilmanshin, R. I. (1991) Study of the 'molten globule' intermediate state in protein folding by a hydrophobic fluorescent probe. *Biopolymers* **31**:119–128.

Seubert, A., Schulein, R. & Dehio, C. (2002) Bacterial persistence within erythrocytes: A unique pathogenic strategy of Bartonella spp. *Int J Med Microbiol* **291**:555–560.

Simon, N. C., Aktories, K. & Barbieri, J. T. (2014) Novel bacterial ADP-ribosylating toxins: Structure and function. *Nat Rev Microbiol* **12**:599–611.

Sixma, T. K., Pronk, S. E., Kalk, K. H., Wartna, E. S., van Zanten, B. A. M., Witholt, B. & Hoi, W. G. J. (1991) Crystal structure of a cholera toxin-related heat-labile enterotoxin from E. coli. *Nature* **351**:371–377.

Slade, D., Dunstan, M. S., Barkauskaite, E., Weston, R., Lafite, P., Dixon, N., Ahel, M., Leys, D. & Ahel, I. (2011) The structure and catalytic mechanism of a poly(ADP-ribose) glycohydrolase. *Nature* **477**:616–622.

Song, J., Gao, X. & Galán, J. E. (2013) Structure and function of the Salmonella Typhi chimaeric A 2 B 5 typhoid toxin. *Nature* **499**:350–354.

Spinelli, S. L., Kierzek, R., Turner, D. H. & Phizicky, E. M. (1999) Transient ADP-ribosylation of a 2'-phosphate implicated in its removal from ligated tRNA during splicing in yeast. *J Biol Chem* 2637–2644.

Stein, P. E., Boodhoo, A., Armstrong, G. D., Cockle, S. A., Klein, M. H. & Read, R. J. (1994) The crystal structure of pertussis toxin. *Structure* **2**:45–57.

Takamura-Enya, T., Watanabe, M., Totsuka, Y., Kanazawa, T., Matsushima-Hibiya, Y., Koyama, K., Sugimura, T. & Wakabayashi, K. (2001) Mono(ADP-ribosyl)ation of 2'-deoxyguanosine residue in DNA by an apoptosis-inducing protein pierisin-1 from cabbage butterfly. *Proc Natl Acad Sci U S A* **98**:12414–12419.

Taupiac, M., Alami, M. & Beaumelle, B. (1996) Translocation of full-length Pseudomonas exotoxin from endosomes is driven by ATP hydrolysis but requires prior exposure to acidic pH. *J Biol Chem* **271**:26170–26173.

Taylor, M., Navarro-Garcia, F., Huerta, J., Burress, H., Massey, S., Ireton, K. & Teter, K. (2010) Hsp90 is required for transfer of the cholera toxin A1 subunit from the endoplasmic reticulum to the cytosol. *J Biol Chem* **285**:31261–31267.

Tsuneoka, M., Nakayama, K., Hatsuzawa, K., Komada, M., Kitamura, N. & Mekada, E. (1993) Evidence for involvement of furin in cleavage and activation of diphtheria toxin. *J Biol Chem* **268**:26461–26465.

Ueno, H., Hohdatsu, T., Muramatsu, Y., Koyama, H. & Morita, C. (1996) Does coinfection of Bartonella henselae and FIV induce clinical disorders in cats? *Microbiol Immunol* **40**:617–620.

Walls, D. & Walker, J. M. (2017) Protein Chromatography. *Protein Chromatogr* **1485**:423.

Wiertz, E. J. H. J., Tortorella, D., Bogyo, M., Yu, J., Mothes, W., Jonest, T. R., Rapoport, T. A. & Ploegh, H. L. (1996) Sec61-mediated transfer of a membrane protein from the endoplasmic reticulum to the proteasome for destruction. *Nature* **384**:432–438.

Wilde, C., Vogelsgesang, M. & Aktories, K. (2003) Rho-Specific Bacillus cereus ADP-Ribosyltransferase C3cer Cloning and Characterization 9694–9702.

Zähringer, U., Lindner, B., Knirel, Y. A., Van Den Akker, W. M. R., Hiestand, R., Heine, H. & Dehio, C. (2004) Structure and biological activity of the short-chain lipopolysaccharide from Bartonella henselae ATCC 49882T. *J Biol Chem* **279**:21046–21054.

Zhang, R. G., Westbrook, M. L., Nance, S., Spangler, B. D., Westbrook, E. M., Scott, D. L. & Shipley, G. G. (1995) The three-dimensional crystal structure of cholera toxin. *J Mol Biol* **251**:563–573.